Journal of Nanobiotechnology

RESEARCH Open Access

Stem cells derived exosome laden oxygen generating hydrogel composites with good electrical conductivity for the tissue-repairing process of post-myocardial infarction

Zhaoyan Xu[1,2], Wanzi Hong[1,2], Yuanxi Mo[1], Fen Shu[1], Yaoxin Liu[1], Yuqi Cheng[1], Ning Tan[1] and Lei Jiang[1*]

Abstract

Acute myocardial infarction (AMI) destroys heart cells by disrupting the oxygen supply. Improving oxygen delivery to the injured area may avoid cell death and regenerate the heart. We present the creation of oxygen-producing injectable bio-macromolecular hydrogels using catalase (CAT) loaded alginate (Alg) and fibrin (Fib) incorporated with the Mesenchymal stem cells (MSCs) derived exosomes (Exo). The composite hydrogel additionally incorporates electrical stimulating qualities from gold nanoparticles (AuNPs). In vitro experiments showed that this composite hydrogel (Exo/Hydro/AuNPs/CAT) exhibits electrical conductivity similar to an actual heart and effectively releases CAT. The O_2_generating hydrogel released oxygen for almost 5 days under hypoxia conditions. We showed that after 7 days of in vitro cell culture, produces the same paracrine factors as rat neonatal cardiomyocytes (RNCs), rat cardiac fibroblasts (RCFs), and Human Umbilical Vein Endothelial Cells (HUVECs), imitating capillary architecture and function. Our work demonstrated that the injectable conductive hydrogel loaded with CAT and AuNPs reduced left ventricular remodeling and myocardial dysfunction in rats after MI. Exo/Hydro/AuNPs/CAT boosted infarct margin angiogenesis, decreased cell apoptosis, and necrosis, and elevated Connexm43 (Cx43) expression. The therapeutic benefits and the ease of production of oxygen make this bioactive injectable conductive hydrogel an effective therapeutic agent for MI.

*Correspondence:
Lei Jiang
jianglei0731@gmail.com

Full list of author information is available at the end of the article

Graphical abstract

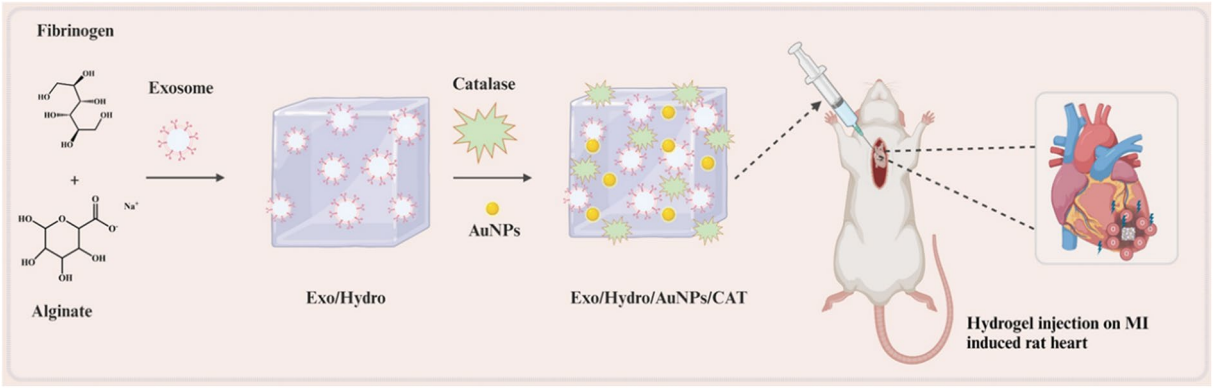

Keywords Au NPs, Catalase, Myocardial infarction, Hydrogel, Exosome

Introduction

Cardiovascular diseases including coronary artery disease, acute myocardial infarction (AMI), and heart failure are a leading cause of death worldwide [1, 2]. Most cardiovascular illnesses lead to heart failure, and myocardial infarction is a leading cause [3, 4]. Endothelial cells cardiomyocytes, cardiac fibroblasts, and may die greatly after an AMI. The absence of oxygen in infarcted tissue is a leading cause of death [5]. In addition to cardiac failure, AMI induces severe pathogenic inflammation. The treatment protects cardiac cells and heals the heart. Clinical reperfusion treatments can achieve these goals by recurring oxygen to the infarcted heart [6, 7]. However, this kind of therapy might not be effective for everyone. While endogenous and exogenous cells can be employed for cardiac healing, they might not survive in the low oxygen atmosphere caused by damaged myocardium. With or without growth factors, biomaterial therapy could encourage myocardial repair by mechanically strengthening cardiac tissue and affecting angiogenesis and inflammation. In the early phases of tissue injury, they cannot give oxygenate metabolically demanding heart cells, limiting their efficacy [8, 9]. Direct oxygen delivery in the infarcted area must be done without harm to protect cardiac cells. However, current oxygen therapy approaches cannot achieve this [10].

Post-AMI tissue microenvironments are inflammatory, with oxidative stress and hypoxia. The pathogenic process, especially acute AMI inflammation, is significantly linked to elevated ROS [11, 12]. Superoxide dismutase, catalase, and small molecular antioxidants monitor ROS production and removal. Elevated ROS levels in the cardiac microenvironment cause myocardial damage. The most frequent ROS following MI is superoxide (O_2^-) and hydrogen peroxide (H_2O_2) [13, 14]. Additionally, abnormal ROS formation will worsen MI tissue inflammation produced by the hypoxic microenvironment. Immune cells, especially macrophages, also shape this microenvironment. Typically, macrophages move from proinflammatory M1 to repair-promoting M2 phenotypes during healing. Nevertheless, high M1 to M2 ratios can aggravate inflammation [6]. Hence, tissue inflammation results from hypoxia, ROS, and inflammatory chemicals such as interleukin-8 (IL-8), interleukin-6 (IL-6), and TNF-α, primarily generated by M1 macrophages. Cell death and tissue damage from chronic inflammation limit infarcted heart repair. In addition to the demand for oxygen in the infarcted region, scarring after MI causes abnormal cardiac electrical transmission [15]. Gold nanoparticles (GNPs) loaded hydrogels could increase cardiomyocyte migration and proliferation and improve post-ischemic function [16].

Stem cells and regeneration biomaterials have improved AMI treatment in the past decade. Stem cells possess numerous limitations, including poor cell preservation, delayed cell preparation, and allogeneic immunological responses. However, regenerative biomaterials like particles, scaffolds, hydrogels, and patches can be used to customize therapeutic performance [17–19]. Direct injection of injectable hydrogels into the infarcted area can treat AMI and restore cardiac function without surgery [20–22]. Hydrogels like calcium alginate, collagen, fibrin, gelatin, etc., inhibit ventricular remodeling and treat myocardial infarction by mechanically supporting the ventricular wall [23, 24]. Growth factors, proteins, drugs, and DNA are applied to biodegradable hydrogels for therapy. Hydrogels are increasingly used to treat MI, but few can change inflammatory microenvironments, which significantly impact treatment outcomes [25]. The blood flow will reduce after AMI and will lead to hypoxic, providing oxygen to the region is the common therapeutic method. Even with inadequate blood supply,

the infarcted area may be able to raise oxygen levels to protect cardiac cells [26, 27]. Thus, heart function may improve. Researchers showed that 100% oxygen-fed dogs had smaller infarcts and better ejection fractions.

Animal models of infarction showed enhanced cardiac cell survival with hyperbaric oxygen. In clinical trials, hyperbaric oxygen therapy enhances cardiac output by 10% and decreases end-systolic volume by 20%. Some treatment trials were less successful [28]. Intracoronary injections of oxygen-rich blood from the artery are a novel method for increasing oxygen concentration in the infarcted area. Numerous clinical trials suggest that patients with significant damage had improved heart function after 30 days. Animal studies investigated how post-MI oxygen carrier blood transfusions affect oxygen saturation [8, 29]. These results show reduced infarct size and improved cardiomyocyte survival. However, this strategy lacks clinical evidence, which is problematic. Focusing on systemic oxygen supply limits MI oxygen therapy [30].

To overcome oxygen delivery limits in MI treatment, we developed an oxygen-generating injectable hydrogel that provides oxygen gradually. We inject a hydrogel into the heart to release oxygen and improve cardiac tissue electrical communication during early myocardial infarction. They also devised a new oxygen delivery method that targets the infarcted area, protecting cardiac tissue and sustaining oxygen supply to metabolically active cardiac cells.

Materials and methods

Materials

Separation of exosomes (EXO)

The Adipose-Derived Mesenchymal Stem Cells (ADMSCs) culture was procured from the ScienCell Research Laboratory and was developed by the Basel medium obtained from STEM Cell Technologies. Cells from the pellet were grown at 37 °C with 5% CO_2 in a medium containing 1% penicillin and 1% streptomycin from Beyotime Biotech in Haimen, China, and 10% FBS from Sigma-Aldrich in St. Louis, MO, USA [31]. Adipogenic, osteogenic, and chondrogenic multilineage differentiation and ADSCs-Exo surface markers (CD 9, CD63, and TSG101) were studied. Western blotting, TEM, and nanoparticle tracking analysis (NTA) also revealed the derivation of exosomes.

Preparation of exo/hydrogel

The sodium salt of alginic acid was used to prepare a 5% alginate solution in sterile calcium-free PBS. The solution was sterilized for 20 min by incubating at 70 °C and cooling to normal conditions. Slowly swirling the solution until completely dispersed produced a viscous solution. A 10% w/v fibrinogen solution was prepared by dissolving the powder in PBS and filtering through a 0.22 µm filter. Stirring rapidly until homogenous, fibrinogen, alginate, and Exosome were mixed in a 10:10:1 ratio. The homogeneous gel was then treated for 15 min in 1 U/mL thrombin solution produced by dissolving thrombin powder in PBS containing 0.1% FBS to polymerize fibrinogen into fibrin before use, thrombin and $CaCl_2$ were filtered through a 0.22 µm filter. The same procedure was performed without exosome to produce Hydrogel alone.

Preparation of Au nanoparticles loaded hydrogel (Exo/Hydro/Au NPs)

The 1.0 g of Exo-Hydro hydrogel was dispersed in the 40 mL of Dichloromethane (DCM) using sonication to obtain a clear solution. The $AuCl_4$ solution with 10% wt, for the Exo-Hydro, was mixed to the dispersion and stirred vigorously until the homogeneous solution. Add 20 mL of 0.1 M $NaBH_4$ aqueous solution to the mixture and stir for 4 h at 60 °C. While the reaction continued in the dual phase, unwanted impurities or ions remained in the aqueous layer. The organic phase with gold nanoparticles in the Exo-hydrogel matrix was carefully recovered.

Preparation of catalase-loaded hydrogels

DMSO (360 µL) was administered sequentially to Exo/Hydro/Au NPs (40 mg), and 1.0 µL CAT (40 mg/mL) under dark circumstances. The final solution contained 10% Exo/Hydro/Au NPs (w/v) and CAT 100 (µg/mL). The combined solution was exposed to UV light for 3s to create Exo/Hydro/Au NPs/CAT hydrogels that scavenge ROS and generate O_2. The same CAT loading procedure was followed on the hydrogel without Au Nanoparticles loading was denoted as Exo/Hydro/CAT.

CAT dispersion in the hydrogel

Crosslinked hydrogel samples were stained with Alizarin red S to ensure equal CAT integration into Hydrogel. The homogeneous gel was then treated for 15 min in 1 U/mL thrombin solution produced by dissolving thrombin powder in PBS containing 0.1% FBS to polymerize fibrinogen into fibrin before use, thrombin and $CaCl_2$ were filtered through a 0.22 µm filter.

Structural observation of hydrogel using a microscope

The hydrogels' microstructures were examined using scanning electron microscopy (SEM), after the following procedures. Hydrogel samples were allowed to be crosslinked, for three days kept in liquid nitrogen to freeze, freeze-dried, and gold-coated.

Evaluation of oxygen-generating kinetics of hydrogel

A ruthenium complex oxygen sensor (Ocean Optics) was utilized to investigate the oxygen release kinetics of hydrogels under hypoxia. 3 mL of medium and 100 U/mL

of catalase loaded with hydrogel were taken in each well of 12 well plates. The plate was then kept in a 1% oxygen incubator.

Evaluation of mechanical properties

The viscoelasticity of the hydrogels with varied proportions was studied using a rheometer (Anton Paar MCR102) with a CP50–1 cone. Time-sweep tests were used to investigate the impact of UV irradiation (6 W UV lamp) at 37°C and 1% strain on hydrogels in terms of storage (G′) and loss moduli (G″). Due to rapid gelation, the test points were fixed as 0.3 s with a frequency of 50 Hz. Additionally, CAT-loaded Hydrogels were subjected to steady and intermittent UV irradiation for 3 s.

Degradation nature of hydrogels

To measure swelling, hydrogels were soaked in PBS for 12 h and weighed electronically. Hydrogels hydrolyzed and had ROS-responsive breakdown in PBS and 250 mM H_2O_2/PBS at 37°C. Daily culture media replacement and hydrogel dry weight (mw) measurement. Degradation was assessed using the mw/me 100% × measure.

In vitro studies

We procured RNCs, HUVECs, and RCFs from the China General Microbiological Culture Collection Center. The obtained cells were grown in Dulbecco's Modified Eagle Medium (DMEM) with 10% fetal bovine serum (FBS) and 1% penicillin-streptomycin. The cultures were incubated with 95% oxygen, and 5% carbon dioxide, with a temperature of 37°C. To cultivate these cells, the Endothelial Cell Growth Kit (Sigma Aldrich, USA) and EGM growth media were mixed to use. Cells from passages 4–7 were studied. High-glucose DMEM media with 1% penicillin-streptomycin with 10% foetal bovine serum were used to grow rat neonatal cardiomyocytes (RNCs).

Cellular uptake assay

For 2 h, 10 mg/mL O_2-generating hydrogels were immersed in 96-well plates with cells to investigate cellular absorption. Cells were stained with Abcam Factin and Sigma 4′,6-diamidino-2-phenylindole (DAPI) after washing, fixing, and blocking. The photos were taken with an Olympus CKX53 fluorescent microscope. The uptake ratio was calculated based on the number of cells that absorbed hydrogel. The cell viability was assessed after absorption. The MTT test ($n \geq 4$) was used to assess RNC viability with the hydrogel group after 2 h of incubation without oxygen release.

Measurement of cellular oxygen

Intracellular oxygen levels were measured after 2 h of lithium phthalocyanine (LiPc) incubation in rat cardiac fibroblasts to increase absorption. The residual LiPc samples were washed three times in DPBS medium. After trypsinization, cells were plated on collagen-coated EPR tubes with or without hydrogels (10 mg/mL) ($n = 3$). After 4 h in a hypoxic incubator (1% O_2, 37°C), EPR tube gas balance was assessed. The tubes were incubated at 1% O_2 for 24 h. EPR spectrum was collected using an X-band Bruker EPR device. By measuring spectrum line width, oxygen % was estimated.

Measurement of cellular ROS content

To assess intracellular ROS, rat cardiac fibroblasts were grown in media with or without CAT hydrogel groups (10 mg/mL; $n = 3$) after pre-staining with H2DCF-DA The photos were taken with an Olympus CKX53 fluorescent microscope. H2DCF-DA positive cell density was compared to normoxia culture conditions for quantification and normalization.

In vitro HUVECs cell migration assay

A 6-well plate contained 90–95% confluent seeded with HUVECs ($n = 3$). The hydrogel groups (10 mg/mL) were added to a medium and scraped the cell monolayer with a pipette tip. At 12 and 24 h, AO-stained cells were observed under an Olympus CKX53 optical microscope. The following equation was used to measure the cell migration ratio (%) with the help of Image J.

$$\text{Migration ratio (\%)} = \frac{\textit{(interval at 0 h) – (interval at 24 h).}}{\textit{interval at 0 h.}} \times 100$$

In vitro tube formation assay of HUVECs cell

HUVECs with a cell density of 8×10^5 cells/mL were grown for 3D collagen gel. Hydrogel groups (10 mg/mL) were added to serum-free media of three cell seeding groups in 1% oxygen. The cells were stained with DAPI and phalloidin 488 after 12 and 24 h and fixed in 4% paraformaldehyde for 45 min. Each group's lumen density was compared to the hydrogel-free control group after phalloidin staining. using a fluorescence microscope.

In vitro gene expression analysis

To produce a 3D culture, rat cardiac fibroblasts were plated at a density of 5×10^5 cells/mL in a collagen gel. Cells were cultured in a medium with or without hydrogel groups at 10 mg/mL under 1% O_2 ($n = 3$). Following the manufacturer's instructions, TRIzol was used to isolate RNA from rat cardiac fibroblasts to assess gene expression. High-capacity cDNA reverse transcription kit synthesized cDNA. The expression of Col1a1, Asma, and Ctgf, genes was evaluated by RT-PCR using SYBR green (Invitrogen) and appropriate primer pairs (Table 1). The

Table 1 Primer sequences used for real-time PCR

mRNA (rat)		Sequence
GAPDH	Forward	5′ TCTCTGCTCCTCCCTGTTCT 3′
	Reverse	5′ TACGGCCAAATCCGTTCACA 3′
Caspase3	Forward	5′ GGAGCAGTTTTGTGTGTGTGA 3′
	Reverse	5′ AGTTTTCGGCTTTCCAGTCAG 3′
Bax	Forward	5′ GCGATGAACTGGACAACAAC 3′
	Reverse	5′ GCAAAGTAGAAAAGGGCAACC 3′
Bcl2	Forward	5′ GGTGGACAACATCGCTCTG 3′
	Reverse	5′ ACAGCCAGGAGAAATCAAACA 3′
CX43	Forward	5′ CTCACGTCCCACGGAGAAAA 3′
	Reverse	5′ CGCGATCCTTAACGCCTTTG 3′
VEGF	Forward	5′ GGGAGCAGAAAGCCCATGAA 3′
	Reverse	5′ GCTGGCTTTGGTGAGGTTTG 3′
Ang-1	Forward	5′ TTCTTCGCTGCCATTCTGACTCAC 3′
	Reverse	5′ GTTGTACTGCTCTGTCGCACTCTC 3′
Collage 1	Forward	5′ TGGATTGCTGGATGAACTT 3′
	Reverse	5′ CTGATGGACCTGACTGAAG 3′
Collage 3	Forward	5′ ACTTGGTTGGCTTGTGA 3′
	Reverse	5′ GTATTATGGTCTGTTCCTGTAG 3′

Actb was used as the housekeeping gene. The data was analyzed using the ΔΔCt method ($n = 4$).

In vivo hydrogel injection into an acute MI model

The study protocol was approved by the Institutional Review Board (or Ethics Com-262 mittee) of Guangdong Provincial People's Hospital (Protocol code Ky-Z-2021-570-01). Lab of Animal Breeding Co., Ltd., China, supplied the male SD rats (8-week-old; 200–250 g). In summary, SD rats were anesthetized for 30 min after receiving 1% sodium pentobarbital (5mL/kg) intraperitoneally. After shaving their upper chests and placing ventilator-connected endotracheal intubation, SD rats got thoracotomies to expose their hearts. The left anterior descending (LAD) coronary artery was ligated with a 6 – 0 silk suture to establish the acute ischemia-induced left ventricular (LV) infarction. Loss of luster and pallid LV myocardium showed the AMI model's success. Using a 30G insulin needle, 50 µL of hydrogel was immediately injected into the damaged myocardial after proper AMI modeling. Both healthy hearts having chest surgery and those with myocardial infarction injected with 50 µL of saline were referred to as the Sham and control groups. Iodine was used to disinfect the experimental sites after chest suturing, and SD rats' oral secretions were treated rapidly to avoid airway obstruction.

Histopathological studies

Rat hearts were taken out on the 28th day, washed with PBS, and stored in formalin (10%) for one whole day before analysis. Through graded alcohol and xylene, paraffin-rooted hearts were sectioned at 3 mm and dewaxed. In PBS, mouse antirat-smooth muscle cell actin was diluted 1:25 to stain mural cells. To detect the primary antibody, goat anti-mouse secondary antibody diluted 1:250 conjugated with an AlexaFluor 488 nm was utilized.

Echocardiography analysis

Multiple groups' cardiac function was examined 28 days following surgery using VisualSonics ultrasonography. When the rats were sedated with isoflurane, 2D transthoracic echocardiography (TEE) in M-mode was conducted to assess their heart function. We measured the rat left ventricle (LV), end-systolic volume (ESV), end-diastolic volume (EDV), fractional shortening (FS), and ejection fraction (EF), to characterize its systolic function and remodelling.

Statistical analysis

Statistics were performed using GraphPad Prism 8.0 (CA, USA). The statistical significance of group differences was assessed using one-way ANOVA. Asterisks (***p, **p, *p) denote statistical significance at $p < 0.001$, < 0.01, and < 0.05. All results are shown as mean ± SD. At least four biological replicates were used in each study.

Results

Synthesis and characterization of hydrogels

We have synthesized an Exosome/alginate/fibrin hydrogel with AuNPs to improve implanted cell survival and prevent hypoxia-related cell death. This hydrogel was modified by adding catalase from the bovine liver (CAT), creating an oxygen-generating Exo/Hydro/AuNPs/CAT (Fig. 1A). The AuNPs were seeded on the hydrogel matrix to increase the conductivity of the composite. The biodegradability, cytocompatibility, and conductivity of the Exo/Hydro/AuNPs/CAT hydrogels were found. The successful intercalation of EXO and CAT on hydrogel was confirmed using Fourier Transform Infrared Spectroscopy (FTIR) analysis. Figure 1B has the FTIR spectra of Exo, CAT, Exo-Hydro, and Exo/Hydro/CAT. The functional group responses such as amide I, amide II, and amide III of exosome proteins were observed in the FTIR spectrum as follows. The peaks at 3331 cm^{-1} and 2898 cm^{-1} are due to the N-H stretching, 1664 cm^{-1} is because of the C-N peptide bond, the peaks at 1561 cm^{-1} and 1297 cm^{-1} are due to the N-H stretching vibrations of amide II, and amide III respectively. The FTIR spectrum of Exo/Hydro has all the peaks responsible for the Exosome in addition to the peaks accountable for the hydrogels at 2940 cm^{-1} for OH stretching, 1715 cm^{-1} is due to the C = O stretching, near 1400 cm^{-1} is because of the OH bending and 1136 cm^{-1} is for the presence of C-O stretching of the molecules Fibrin and Alginate present in the hydrogel. The FTIR spectrum of CAT has a peak around 3477 cm^{-1}, 3629 cm^{-1}, and 2957 cm^{-1} due to the stretching vibration of the OH group and

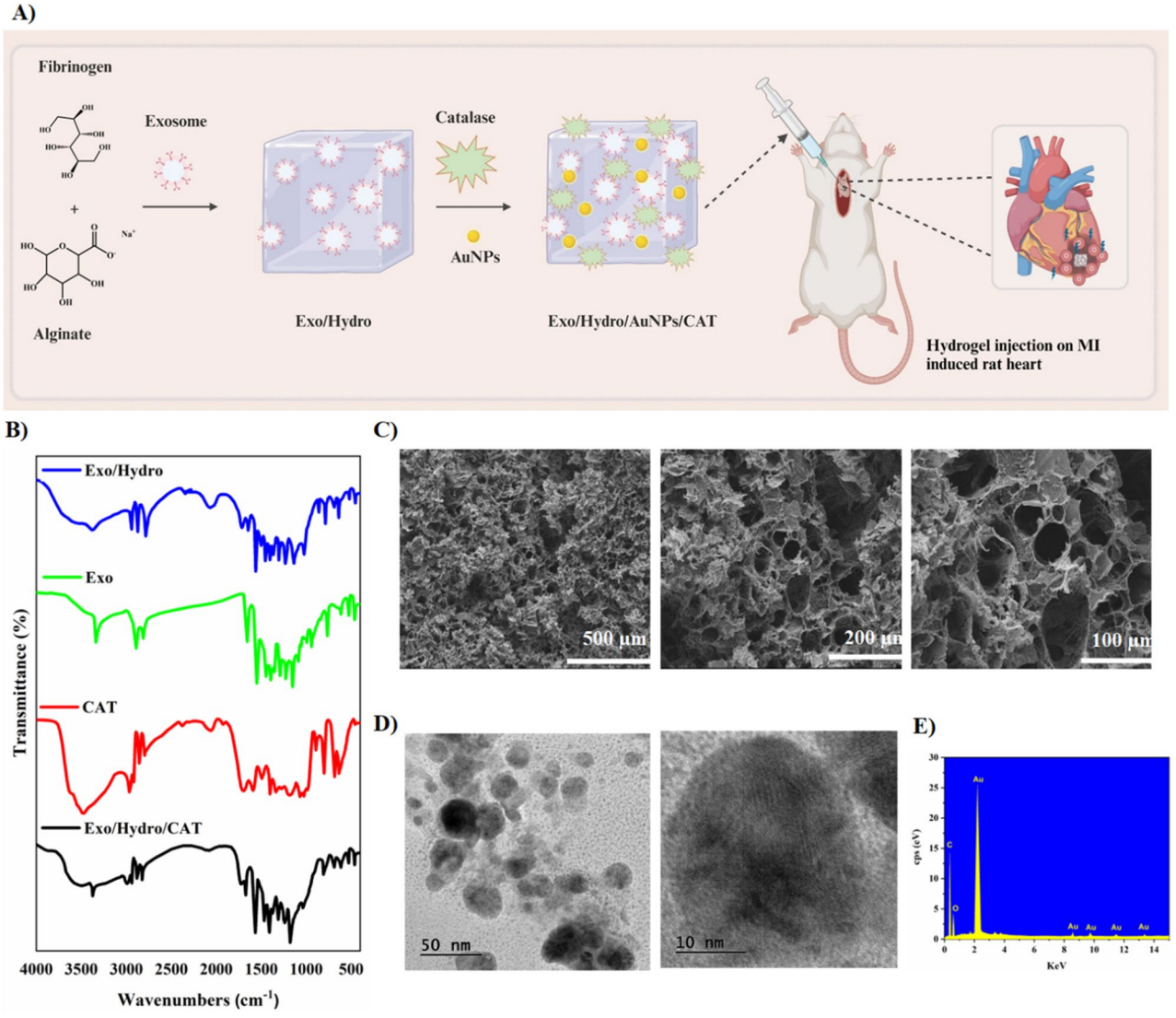

Fig. 1 Schematic representation of the synthesis of Exo/Hydro/AuNPs/CAT injectable hydrogel and their therapeutic procedure for acute myocardial infarction (**A**). Physicochemical characterization of hydrogel composites; (**B**) FT-IR spectrum of Exo, CAT, Exo/Hydro, and Exo/Hydro/CAT; (**C**) SEM images of Exo/Hydro/AuNPs/CAT with different magnifications; (**D**) HR-TEM images of Exo/Hydro/AuNPs/CAT with different magnifications; (**E**) EDAX result of Exo/Hydro/AuNPs/CAT

a peak around 1374 cm $^{-1}$ due to OH group bending, respectively. The peaks around 1706 cm $^{-1,}$ 1204 cm $^{-1,}$ 1161 cm $^{-1,}$ and 790 cm $^{-1,}$ are due to the C = O stretching, C-O stretching, C-N stretching, and C = C bending vibrations respectively. The Exo/Hydro/CAT composite has the combined peaks responsible for the Exo, CAT, and the hydrogels observed in the earlier spectra, which infers the successful formation of the composite with Exo, Hydro, and CAT. The hydrogel's morphology was validated by SEM. Figure 1C shows the homogenous porosity hydrogel. Figure 1D shows HR-TEM analysis confirming the homogeneous dispersion of Au nanoparticles on the hydrogel. The average particle size of the AuNPs was measured as 25 nm (Fig. 1D) and the elemental presence of Au was confirmed using EDAX analysis (Fig. 1E). The TEM image shows the Exo derived from the AD-MSCs has a nearly spherical morphology, and the average diameter of the Exo was detected as 130 nm by Flow Nano Analyzer (Figure SI 1A, C). Exosomes retain the lipid and protein content of the parent cells in addition to their distinct membrane characteristics. Some of the protein markers found in exosomes are thought to be peculiar to exosomes, such as CD63, TSG 101, and CD9 [32]. Consequently, western blot analysis was carried out to validate the existence of these exosome markers. Exosomes isolated from AD-MSC lines and whole cell lysate both included the CD63, TSG 101, and CD9 proteins, as shown in Figure SI 1B.

The gelation efficiency is one of the important parameters of an effective hydrogel. The gelation time of the

hydrogel was studied using a rheometer as depicted in Fig. 2A. The gelation time of the Exo/Hydro was observed around 200 s and the same was reduced a little bit for Exo/Hydro/CAT and Exo/Hydro/AuNPs/CAT. The rheometer graph also shows a parallel upregulation pattern with CAT and AuNPs, which were used to calculate the mechanical strength of the materials. Figure 2B demonstrates that the gelation process took about 4 min, forming the Exo/Hydrogel in 226 ± 3 s. The gelation response was faster such as 185 ± 3 s and 180 ± 4 s, when CAT and AuNP were introduced (Fig. 2B). The hydrogels' mechanical strength was measured with a rheometer as described in the materials and method section. Figure 2C shows the modulus of Exo/Hydro, Exo/Hydro/CAT, and Exo/Hydro/AuNPs/CAT hydrogels, which shows that the mechanical strength was observed with an increasing trend after the introduction of AuNPs and CAT. Figure 2D shows that all hydrogels have stable curves between 1.1 and 100 rad/s. It is familiar that, AuNPs could improve the conductivity of the

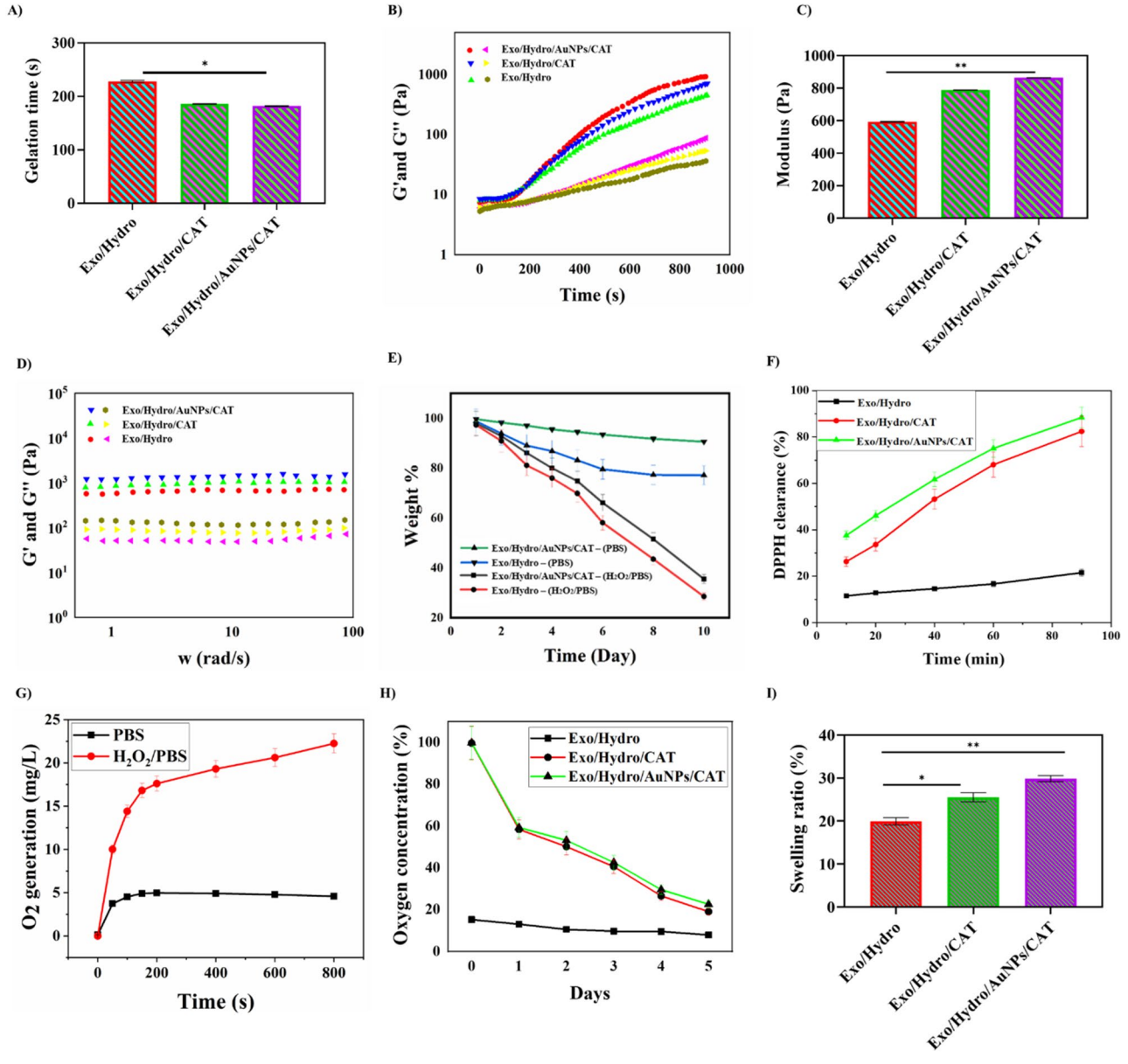

Fig. 2 Mechanical and therapeutic properties of hydrogel composites; (**A**) Gelation time of various hydrogel composites; (**B**) Rheological behaviour of the hydrogels; (**C**) Modulus of various hydrogels; (**D**) The frequency-scan curves of the hydrogels; (**E**) Degradation properties of various hydrogels in PBS and H_2O_2/PBS medium; (**F**) DPPH clearance analysis of developed hydrogel groups in 100 µm H_2O_2/1 m KI solution and time prolongation; (**G**) The O_2 generation properties of Exo/Hydro/AuNPs/CAT in PBS and H_2O_2/PBS conditions; (**H**) Oxygen release kinetics under anoxic condition of prepared various hydrogels; (**I**) swelling ratio of different hydrogels. *$p < 0.05$, **$p < 0.01$

nanocomposites due to their electronic structure [33]. In this work, we have also identified that the hydrogel composite's electrical conductivity was increased after being loaded with AuNPs (Table 2). The Exo/Hydro/AuNPs/CAT hydrogel has a conductivity of 8.51×10^{-4} S/cm that is similar to the natural myocardial range of 5×10^{-5} to 1.6×10^{-3} S/cm, hence the as-synthesized hydrogel could be employed to treat myocardial infarction.

Table 2 The conductivity of Exo/Hydro; Exo/Hydro/CAT, Exo/Hydro/AuNPs/CAT hydrogel and Native myocardium tissue

Samples	Conductivity (S/cm)
Exo/Hydro/AuNPs/CAT	$8.51 \pm 0.18 \times 10^{-4}$
Exo/Hydro/CAT	$9.53 \pm 0.41 \times 10^{-5}$
Exo/Hydro	$8.78 \pm 0.18 \times 10^{-5}$
Native myocardium tissue	$\approx 10^{-4}$

Degradation property and therapeutic efficiency of hydrogels

The degradation properties of the Exo/Hydro and Exo/Hydro/AuNPs/CAT hydrogels were studied from the change in the weight in 250 mM of H_2O_2/PBS and PBS solutions. The mass of Exo/Hydro and Exo/Hydro/AuNPs/CAT hydrogels were reduced significantly in both solutions compared to the original solution (Fig. 2E). When exposed to 250 mM H_2O_2/PBS and PBS, the Exo/Hydro and Exo/Hydro/AuNPs/CAT hydrogels lost 70% and 30% of their weight, respectively. The noticed reduction in PBS is due to hydrolysis affecting β-amino ester bonds. The Exo/Hydro/CAT and Exo/Hydro/AuNPs/CAT hydrogels showed a 75% reduction in DPPH in 90 min, as shown in Fig. 2F. Conversely, the Exo/Hydro hydrogel did not successfully eliminate DPPH, except that the other two hydrogels effectively eliminated H_2O_2 (Fig. 2F). The Exo/Hydro/CAT hydrogel's efficiency in producing O_2 was displayed through its immersion in 50 mM H_2O_2/PBS and PBS (Fig. 2G). Only the H_2O_2/PBS solution had gas bubbles, not PBS. Figure 2H shows that the 50 mM H_2O_2/PBS solution's oxygen (O_2) content increased gradually over 800 s. On the other hand, PBS solution hypoxia remained steady. The CAT in the Exo/Hydro/CAT and Exo/Hydro/AuNPs/CAT hydrogels converted extra hydrogen peroxide (H_2O_2) into oxygen (O_2) without losing its efficiency. This particular trait is useful in inflammatory tissue milieus like myocardial infarction.

This work shows that Exo/Hydro scavenges ROS and CAT converts H_2O_2 into oxygen in the hydrogel, and the AuNPs increase the electrical conductivity of the hydrogel composite. These effects regulate cardiac microenvironments with high ROS and hypoxia, improving myocardial infarction treatment. To study oxygen release kinetics in an Exo/Hydro, Exo/Hydro/CAT, and Exo/Hydro/AuNPs/CAT hydrogel were separately added to a 12-well. An oxygen sensor measured the media with dissolved oxygen for five days. A sealed container built for hypoxic environments to conduct experiments in controlled parameters with low oxygen levels. Purging the container with N_2 gas maintained a hypoxic environment. As expected, the hydrogels without CAT sustained an oxygen content of roughly 0% throughout the experiment (Fig. 2H). The dissolved oxygen content of the hydrogels with CAT-functionalized hydrogels was found very less during the initial state. Also, it is observed that the Exo/Hydro alone cannot produce oxygen. Hydrogels with CAT can release oxygen continuously for five days. Once encapsulated in the hydrogel's aqueous environment, oxygen content increased significantly, reaching 100%.

Despite the fast and extensive release, Exo/Hydro/CAT, and Exo/Hydro/AuNPs/CAT could raise oxygen tension to 16% in one day, 14% in three days, and 7% in five days. CAT's high response rate leads to a rapid decrease in oxygen generation, causing the observed release curve to fall. The Exo/Hydro/CAT, and Exo/Hydro/AuNPs/CAT hydrogels created an oxygen-rich microenvironment for at least five days. The swelling behavior of the various hydrogels was studied as per the procedure given in the material and method section. The swelling ratio of the hydrogels with CAT was found higher than the one without CAT (Exo/Hydro). The swelling ratios of Exo/Hydro, Exo/Hydro/CAT, and Exo/Hydro/AuNPs/CAT are as follows; 19 ± 0.3, 24 ± 0.4, and 29 ± 0.5 (Fig. 2I). The results match expectations since CAT increases water permeability and cross-linking density controls hydrogel swelling.

Evaluation of in vitro activities of hydrogels

Hypoxia in infarcted hearts causes widespread cardiac cell death as given in Fig. 3A. We incubated human umbilical vein endothelial cells (HUVECs), rat cardiac fibroblasts (RCFs), and rat neonatal cardiomyocytes (RNCs) with Exo/Hydro, Exo/Hydro/CAT, and Exo/Hydro/AuNPs/CAT in serum-free media under 1% oxygen for five days to determine their potential to enhance cell viability. Endothelial, cardiomyocyte, and cardiac fibroblast cells are vital to repair heart damage. The Exo/Hydro hydrogel without oxygen-generating capacity was used to compare the activity of the hydrogel incorporated with CAT. Double-stranded DNA (dsDNA) was measured to determine cell count. After five days in cultivation without oxygen, all three cell types died significantly (Fig. 3B, C & D). Interestingly, Exo/Hydro/CAT, and Exo/Hydro/AuNPs/CAT hydrogel groups release oxygen, boosting cell survival.

To study the internalization of the Exo/Hydro/AuNPs/CAT hydrogel by endothelial cells, cardiomyocytes, and macrophages, the hydrogel was incubated with macrophages, HUVECs, and RNCs. After a 2-hr incubation,

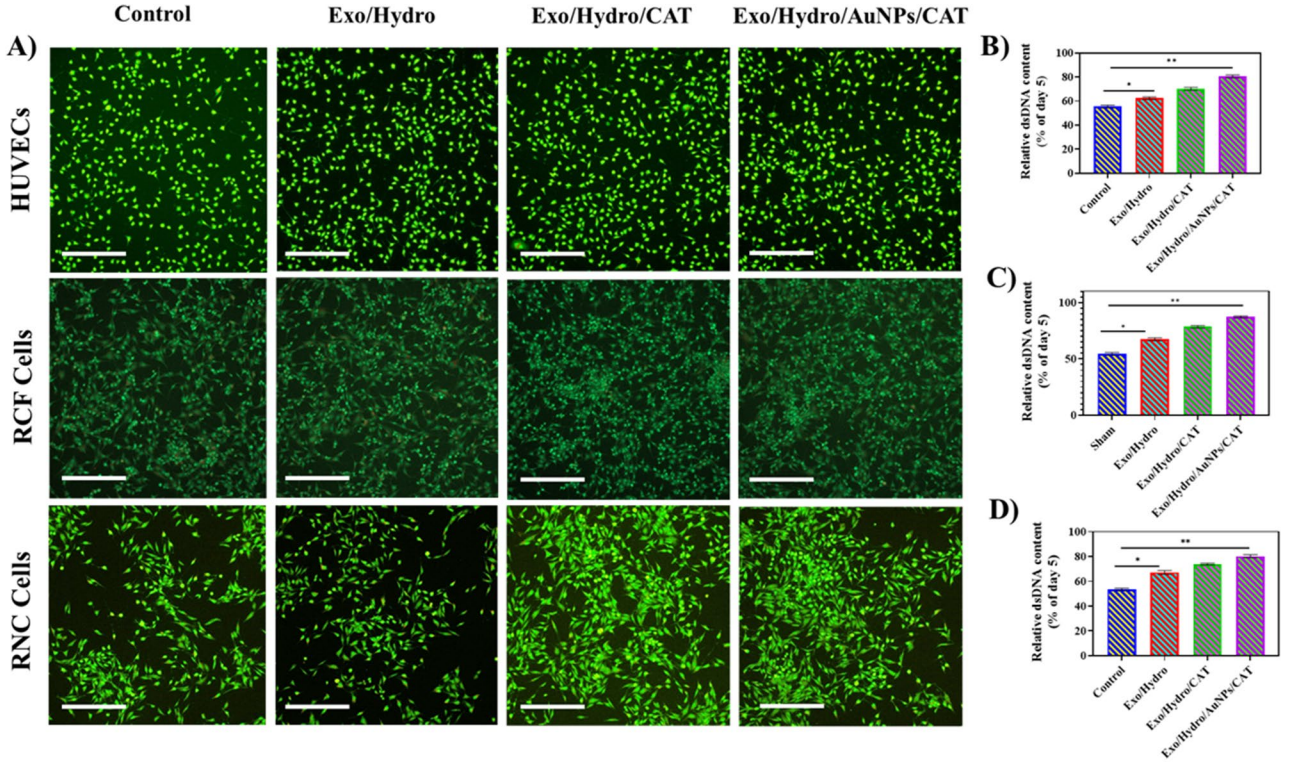

Fig. 3 In vitro cell compatibility behaviors of synthesized various hydrogels on HUVECs, RCF cells, and RNC cells. (**A**) Morphological observation of cells treated with various hydrogel composites under fluorescence microscopy (Calcein-AM staining. Scale bar = 100 μm); (**B**, **C**, **D**) In vitro quantitative measurements of relative dsDNA content of HUVECs, RCFs, and RNCs treated with hydrogel groups for 5 days culture. *$p < 0.05$, **$p < 0.01$

34% of RNCs, 15% of HUVECs, and 24% of macrophages internalized the Exo/Hydro/AuNPs/CAT hydrogel (Fig. 4A). The Figure shows that the Exo/Hydro/AuNPs/CAT hydrogel did not affect mitochondrial viability in RNCs. We used electron paramagnetic resonance (EPR) to measure intracellular oxygen content. The cellular oxygen content of cardiac fibroblasts grown in a medium depleted of oxygen and added with hydrogels was 4.9% after 24 h of incubation at a 1% oxygen environment. As seen in Fig. 4B, Exo/Hydro/AuNPs/CAT hydrogel increased cellular oxygen to 13.4%. To survive in hypoxic conditions, cells need oxygen to produce ATP. Figure 4C shows an ATP test to measure HUVECs' cellular ATP levels under hypoxic conditions, which inferred that the introduction of oxygen increased ATP levels in HUVECs. The excessive production of reactive oxygen species (ROS) during oxygen delivery to cells might cause cellular death. We measured cellular ROS levels after administering three hydrogels to cardiac fibroblasts under hypoxic circumstances for 5 days to evaluate if released oxygen could cause excessive ROS formation. Incubation with hydrogels increased cellular ROS compared to hypoxia-only. Nevertheless, this spike was not significantly different related to normoxia-cultured cells (Fig. 4F). These findings imply that released oxygen had no significant impact on ROS generation.

Vascularization helps heart tissue recover from myocardial infarction. Our idea was that increased oxygen levels in cells would increase their survival under hypoxic conditions. Two processes regulate hypoxia-induced cardiac cell death: apoptosis or necrosis. In general, though apoptosis is unfavorable, necrosis is worse since it damages nearby cells and tissues. Flow cytometry revealed that the Exo/Hydro group with no oxygen generation had double the mortality rate due to necrosis (24.9 ± 6.5%) as compared to apoptosis (8.1 ± 4.2%) (Fig. 4G). The introduction of Exo/Hydro/CAT and Exo/Hydro/AuNPs/CAT groups significantly reduces necrosis and apoptosis, increasing cell viability. The decrease in O_2-induced necrotic cells correlated with an increase in surviving cardiac cells. We measured cardiac cell lactate dehydrogenase (LDH) excretion to confirm the unexpected decrease in necrosis from O_2 production (Fig. 4E).

We used HUVECs to undertake an in vitro endothelial tube creation assay, and cell migration test to see if oxygen produced under hypoxic circumstances may drive vasculogenesis. HUVEC migration increased significantly with Exo/Hydro/CAT and Exo/Hydro/AuNPs/CAT groups, as given in Fig. 5(A & B). The migration ratio of HUVECs in the Exo/Hydro/CAT and Exo/Hydro/AuNPs/CAT groups was roughly twofold higher after 24 h of culture than in the Exo/Hydro group. Similarly,

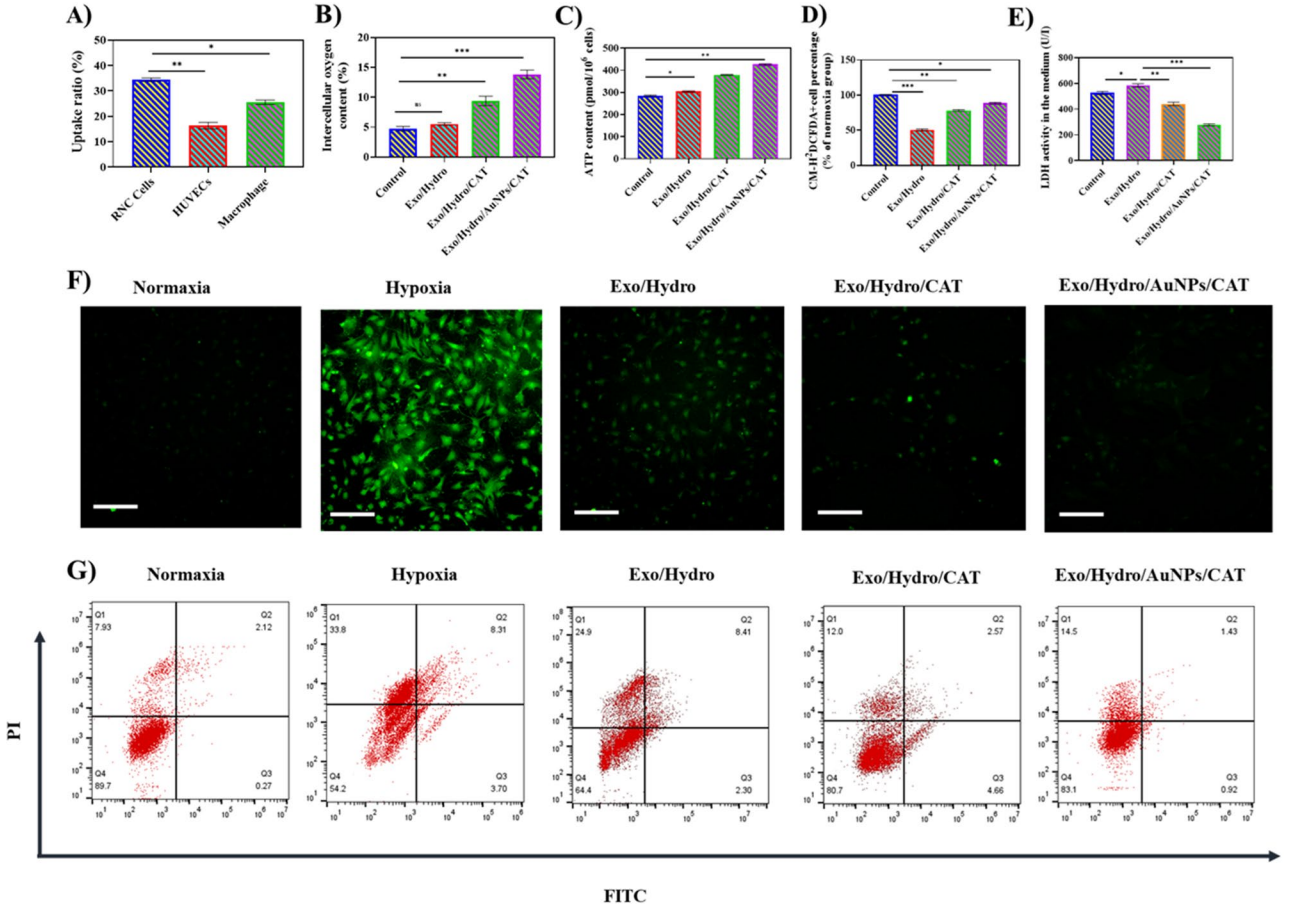

Fig. 4 In vitro qualitative and quantitative analysis of various hydrogels. (**A**) Cellular uptake ratio of hydrogel with different cell types (RNCs & HUVECs & Macrophages); (**B**) intracellular oxygen content in RCFs; (**C**) intracellular ATP content with various hydrogel groups in HUVECs; (**D**) quantitative analysis of ROS content in RCFs (DCF-DA staining); (**E**) LDH activity of various hydrogels; (**F**) Qualitative analysis of ROS content in RCFs under normoxia and hypoxia environments treated with various hydrogel groups under fluorescence microscope (scale bar = 100 μM) (**G**) In vitro cell apoptosis analysis on RNCs under normoxia and hypoxia microenvironments using flow cytometry method (FITC and PI staining).*$p < 0.05$, **$p < 0.01$, ***$p < 0.001$

Exo/Hydro/AuNPs/CAT hydrogel treatment increased endothelial lumen development. This rise was 2.5 times greater than in the control group (Fig. 5C). Oxygen release by the CAT-incorporated hydrogels accelerates endothelial tube development (Fig. 5(C & D)) in infarcted hearts under the situation of very low oxygen and nutrient availability. Improved cell survival and migration may be the cause for this enhancement. We cultured cardiac fibroblasts in a three-dimensional collagen gel with 1% oxygen to analyse if oxygen release could inhibit myofibroblast development [8]. After treating the culture media with TGFβ1, two groups were created: one with an oxygen-releasing (CAT) hydrogel and the other without CAT. As shown in Fig. 5E and Figure SI 2, CAT-incorporated hydrogels such as Exo/Hydro/CAT and Exo/Hydro/AuNPs/CAT used treatment decreased the number of cardiac fibroblasts that differentiated into myofibroblasts. The Exo/Hydro/CAT and Exo/Hydro/AuNPs/CAT hydrogel groups had significantly lower mRNA levels of myofibroblast markers like Asma, Ctgf, and Col1a1 (Fig. 5F). The study found that oxygen-releasing nanoparticles successfully reduced myofibroblast growth in a hypoxic environment.

Evaluation of heart function after hydrogel injection

We examined heart function at various periods after hydrogel injection using hemodynamic testing or echocardiography at the end of the research. After 4 weeks of myocardial infarction, rats showed delayed left ventricular segmental wall movement poor myocardial contractility, reduced wall thickness, and expanded left ventricular cavity in an M-type mode. Direct injection of hydrogels to some extent repaired these defects. In particular, the Exo/Hydro/CAT and Exo/Hydro/AuNPs/CAT groups had nearly normal cardiac function (Fig. 6). After left coronary artery ligation, long-axis images showed that LVAWs and LVPWs gradually decreased, LVIDs and LV Vols increased, and LVEF and LVFS considerably decreased (Fig. 6A to F). Hydrogel injection improved all these cardiac dysfunctions, but the one loaded with CAT

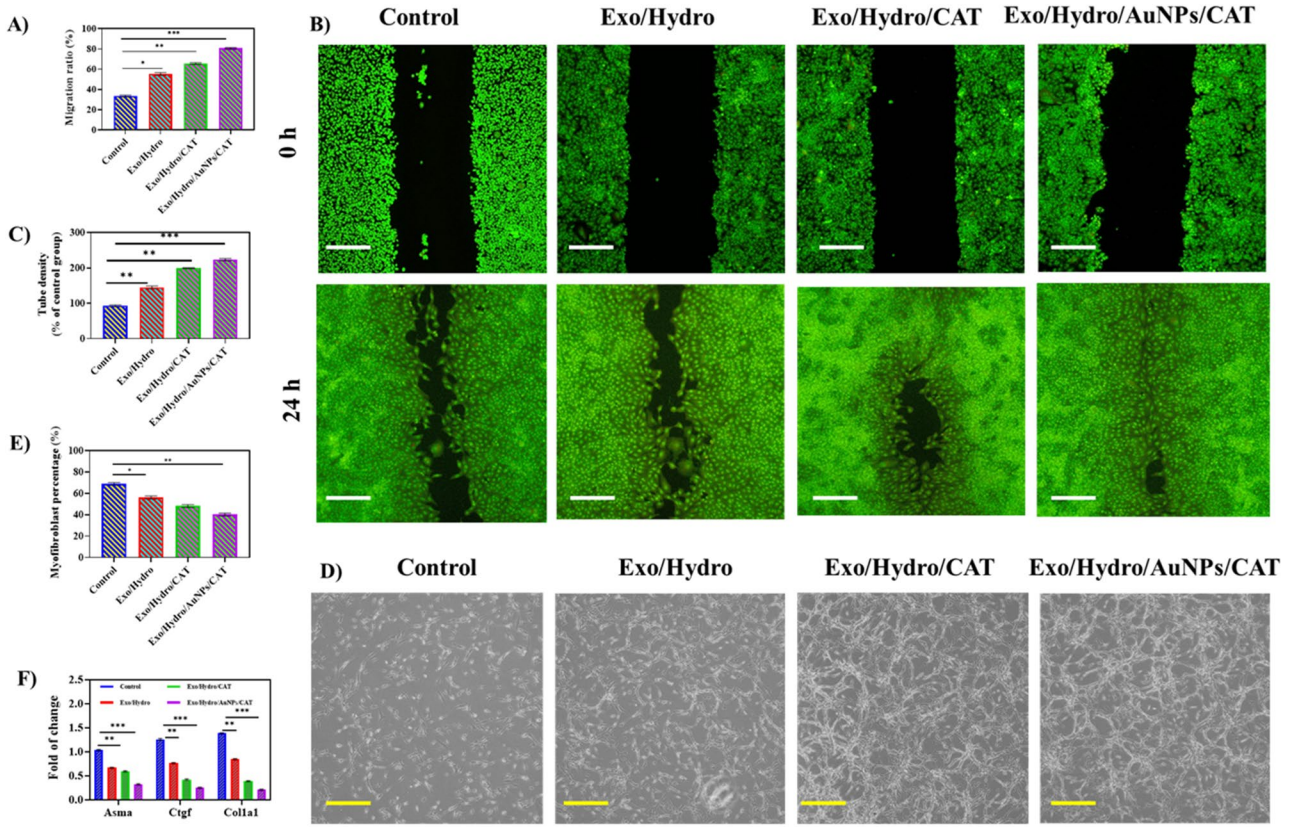

Fig. 5 In vitro evaluation of migration, tube formation, myofibroblast percentage calculation. (**A**, **B**) Quantification and qualification of cell migration ratio (%) on HUVECs cells using AO staining treated with various hydrogels for 0 and 24 h (scale bar = 100 μM); (**C**, **D**) quantification of endothelial cells tube formation and fluorescence images for tube formation for 0 and 24 h with various hydrogels under fluorescence microscopic method (scale bar = 100 μM); (**E**) quantification of αSMA positive myofibroblast density on RCFs treated with different hydrogel groups and cultured on collagen gels for 24 h; (**F**) relative gene expression analysis of Asma, Ctgf and Col1a1 in RCFs treated with different hydrogel groups for 24 h. *$p < 0.05$, **$p < 0.01$, ***$p < 0.001$

and AuNPs had the most benefit. After 2 weeks of treatment, LVIDs and LV Vols in the Exo/Hydro/AuNPs/CAT, and Exo/Hydro/CAT groups were significantly lower than those in the AMI group (3.21 ± 0.72 vs. 4.16 ± 0.1272 vs. 4.94 ± 0.16; 159.21 ± 6.17 vs. 184.5 ± 5.18 vs. 245.1 ± 3.21), while LVAWs, EF, and FS were significantly higher (2.12 ± 0.61 vs. 1.89 ± 0.13 vs. 1.05 ± 0.12; 50.92 ± 0.42 vs. 35.84 ± 0.45 vs. 25.89 ± 0.41). Doppler was used to assess AV peak Vel, E/A, and cardiac output (CO) four weeks after surgery (Fig. 7A-C). Both the CAT-loaded hydrogels, Exo/Hydro/CAT (964.48 ± 35.41; 0.03 ± 0.14; 59.84 ± 0.56) and Exo/Hydro/AuNPs/CAT (933.57 ± 3.41; 1.04 ± 0.05; 62.88 ± 0.57) have greater parameters than the MI group. However, the Exo/Hydro and MI groups show comparable values in these parameters. Treatment with Exo/Hydro/AuNPs/CAT resulted in increased E/A values for rats compared to the AMI group (1.043 ± 0.03 vs. 0.64 ± 0.02), as seen in Fig. 7A-C. The hemodynamic analysis results are displayed in Fig. 7D-F. In contrast to the sham group, MI rats exhibited notable declines in load-dependent markers such as LVSP and ± dp/dt max. Treatment with Exo/Hydro/AuNPs/CAT or Exo/Hydro/CAT improved the parameters LVSP and ± dp/dt max in rats with MI. However, the Exo/Hydro group showed parameters that were comparable to the MI group. Compared to the Exo/Hydro group, the LVSP and + dp/dt max of the Exo/Hydro/AuNPs/CAT group were considerably higher (98.83 ± 1.56 vs. 70.67 ± 1.63; 5991.63 ± 60.51 vs. 5006.82 ± 30.12). The data indicate that hydrogels loaded with CAT and AuNPs may improve cardiac functions in rats with MI more broadly and efficiently.

Evaluation of pathological changes, fibrosis and apoptosis in myocardial tissue after hydrogel injection

The MI group changed morphologically. Transverse striations were torn, cell-cell interaction was disturbed, nuclei were unevenly condensed or disintegrated, and inflammatory cell infiltration increased. The heart sectioning images of H&E-stained myocardium show that the infarcted regions of AMI were reduced in the Exo/Hydro, Exo/Hydro/CAT, and Exo/Hydro/AuNPs/CAT treated groups as shown in Fig. 8A. The infarcted region treated with Exo/Hydro/AuNPs/CAT hydrogel showed the greatest improvement in resisting pathological and

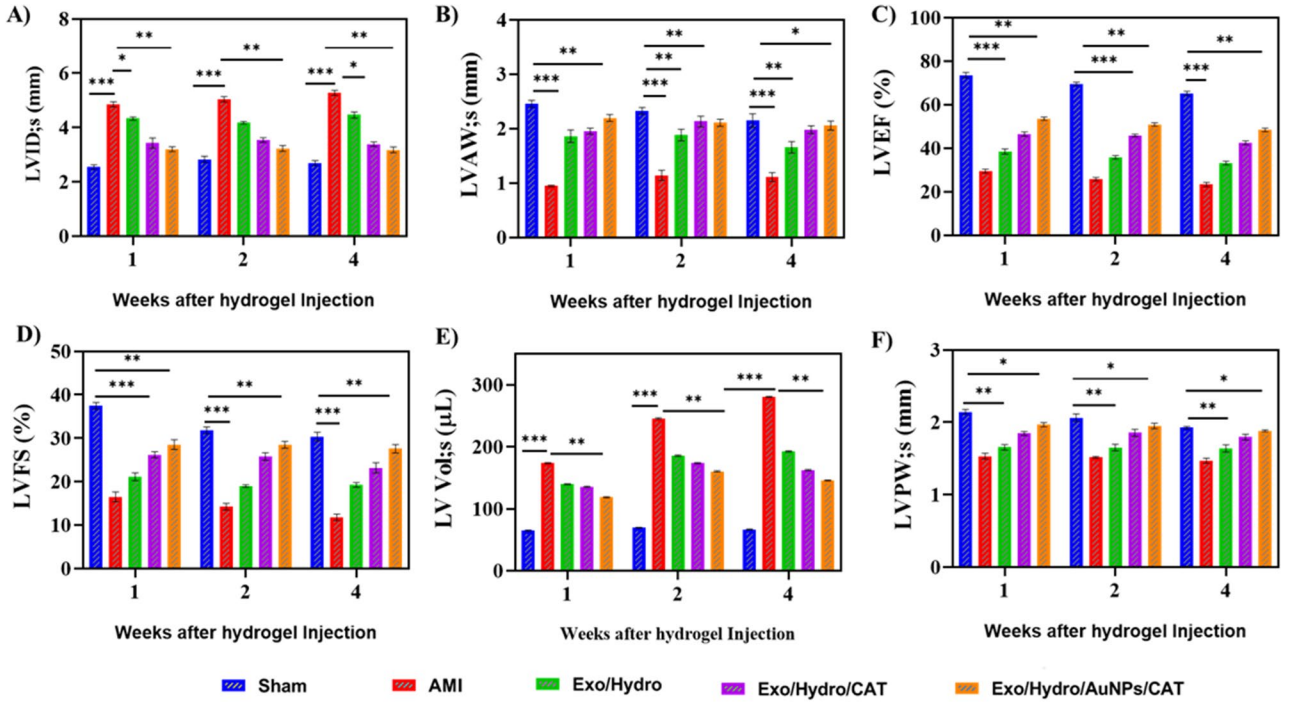

Fig. 6 Evaluation of cardiac functions in various groups. (**A**-**F**) Presented are the time courses of LVID; s, LVAW; s, LVEF, LVFS, LV Vol; s, and LVPW; s versus sham group; versus MI group.*$p < 0.05$, **$p < 0.01$, ***$p < 0.001$

morphological alterations. After MI, Masson trichrome staining showed collagen buildup (blue) at the infarction edge (Fig. 8B). The quantitative results indicated that MI rats had considerably higher myocardial infarction ratio (%), and lower wall thickness, which may be improved by several therapies. Compared to the other two treatment groups, rats treated with Exo/Hydro/AuNPs/CAT only demonstrated a drift to a reduction in myocardial infarction ratio and increment in the wall thickness after 4 weeks post-AMI compared with other groups (Fig. 8C, D). We hypothesize that the measuring time point may explain the lack of variation in cardiac fibrosis area between treatment groups. These results match functional data. Hydrogel containing CAT and AuNPs reduces fibrosis and improves cardiac function.

Evaluation of apoptosis in myocardial tissue after hydrogel injection

Apoptosis controls cardiac damage and left ventricular remodeling after MI [34, 35]. The MI group considerably increased cell apoptosis, while the sham surgery group had essentially little TUNEL-positive signal (Figure SI 3 A, B). MI-induced myocardial apoptosis in rats was reduced by hydrogel. CAT and AuNPs hydrogels inhibited MI-induced cell apoptosis better than Exo/Hydro. Apoptosis is a cell death process that involves several signaling channels and genetic regulation (Figure SI 3D-I). The study found that following MI, Bcl2 expression reduced (0.66 ± 0.01 vs. 0.31 ± 0.02), but Bax expression rose (0.54 ± 0.01 vs. 1.24 ± 0.02). Hydrogel alone may mitigate this shift. Hydrogel with CAT and AuNPs led to enhanced Bcl2 expression (0.75 ± 0.21 vs. 0.31 ± 0.02) and decreased Bax protein expression (0.63 ± 0.02 vs. 1.24 ± 0.02), resulting in a lower Bax/Bcl2 ratio. Protein ATP5d is involved in energy metabolism. MI reduced ATP5d expression, although Exo/Hydro/AuNPs/CAT or Exo/Hydro/CAT restored it. Exo/Hydro did not affect ATP5d. The Exo/Hydro/AuNPs/CAT group showed considerably increased expression of ATP5d and Bcl2 compared to the Exo/Hydro (1.03 ± 0.02 vs. 0.76 ± 0.21; 0.75 ± 0.21 vs. 0.42 ± 0.02), but Bax/Bcl2 was dramatically reduced (0.54 ± 0.01 vs. 1.05 ± 0.02). An important apoptotic signalling molecule is caspase 3. Compared to the sham group, MI significantly increased Caspase3 and cleaved Caspase3 expression (0.54 ± 0.01 vs. 1.22 ± 0.01; 0.84 ± 0.21 vs. 1.66 ± 0.01), while all treatment groups showed a significant downregulation of Caspase3. However, Exo/Hydro/CAT and Exo/Hydro/AuNPs/CAT treatment significantly reduced cleaved Caspase3 levels relative to the MI group (Figure SI 3 H and I). The data showed that CAT and AuNPs loaded hydrogels reduced MI-induced cardiac dysfunction by reducing apoptosis.

Evaluation of neovascularization and transcriptional level in myocardial tissue after hydrogel injection

Collateral circulation helps in restoring blood supply to injured heart tissues after MI [36]. Cx43 is a crucial protein that forms the gap junction channel between

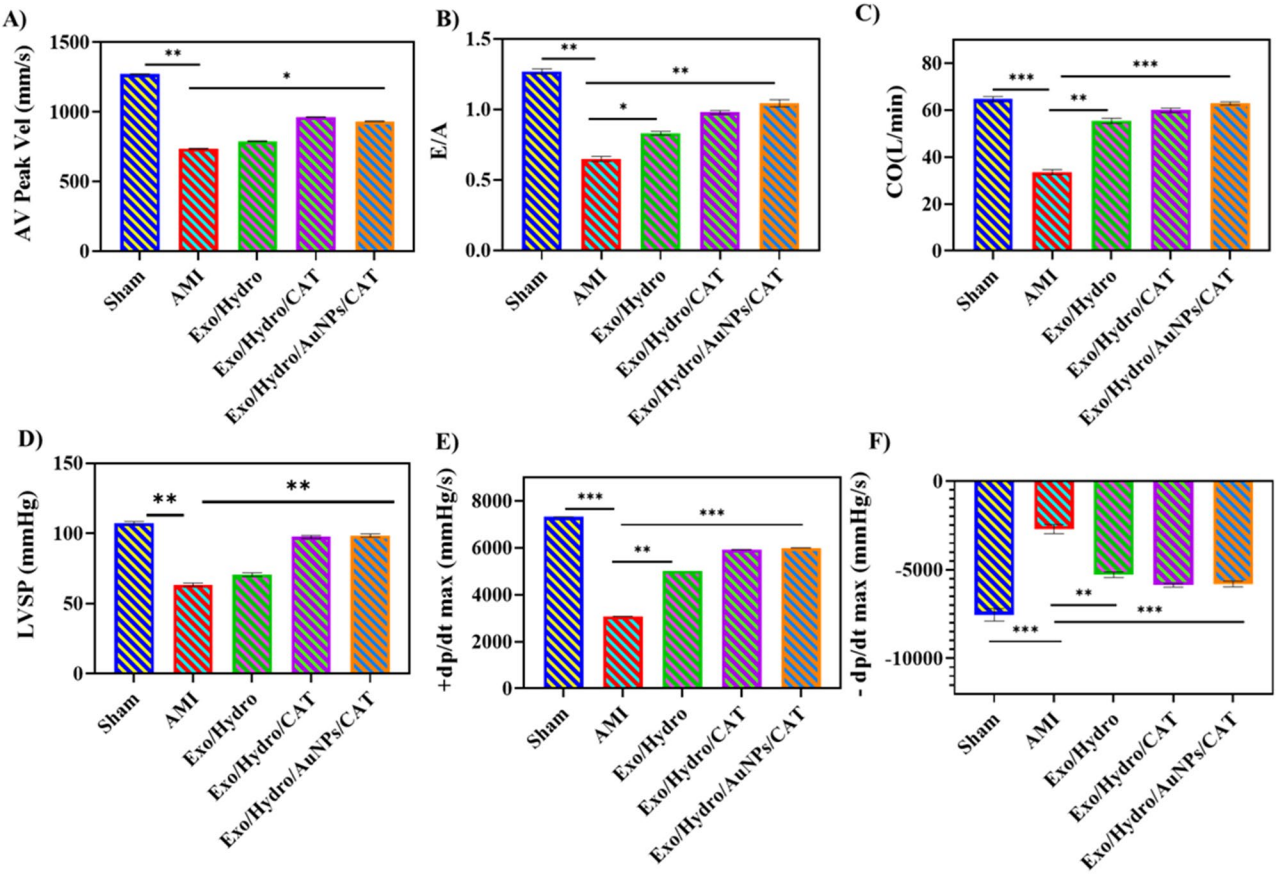

Fig. 7 Evaluation of hemodynamics in various groups. (**A**-**C**) Quantitative assessment of cardiac diastolic function based on AV Peak Vel, E/A and CO. (**D**-**F**) Quantitative assessment of hemodynamics on cardiac function based on LVSP, +dp/dtmax, and − dp/dtmax. *$p < 0.05$, **$p < 0.01$, ***$p < 0.001$

ventricular myocytes. It enhances cardiomyocyte signaling and electric current transmission [37]. Cx43 promotes cell-cell connections via ion channels, ensuring a steady ionic conduction rate and direction [38]. Hydrogels restored Cx43 expression after MI (Figure SI 4 A & B). In particular, Cx43 expression was substantially higher in the Exo/Hydro/AuNPs/CAT group than in the Exo/Hydro group and it is comparable with the Exo/Hydro/CAT group (Figure SI 4B). Our findings suggest that promoting electrical signal coupling between cardiomyocytes or between cardiomyocytes and fibroblasts may lead to synchronized contraction and improve cardiac function.

We used RT-PCR to identify MI problematic transcription factors after hydrogel therapy. These genes include, Bax, Bcl2, and Caspase3 for apoptosis, VEGF and Ang-1 for angiogenesis, collagen type 1 and 3 for fibrosis, and Cx43 for cardiac tissue electrical and mechanical coupling. In the marginal zone of myocardial infarction, collage 1 and 3 mRNA expression were considerably greater in the MI group compared to the sham group (1.89 ± 0.45 vs. 54.38 ± 1.62; 1.63 ± 0.23 vs. 14.74 ± 1.72). After 4 weeks of hydrogel injection alone, collage 3 mRNA expression was considerably decreased, whereas collage 1 mRNA was unaffected (Figure SI 4 C).

Hydrogel-loaded CAT or AuNPs significantly reduced collage 1 or 3 transcription levels, with the Exo/Hydro/AuNPs/CAT group showing the greatest effect, with collage 1 mRNA levels significantly lower in rats' myocardial tissue (12.01 ± 1.72 vs. 33.56 ± 0.75). MI group had the lowest VEGF and Ang-1 mRNA levels. The Exo/Hydro/AuNPs/CAT strongly increases VEGF mRNA and Ang-1 (Figure SI 4D). Exo/Hydro/AuNPs/CAT significantly increase VEGF and Ang-1 mRNA levels, with VEFG mRNA levels significantly higher than the Exo/Hydro group (0.46 ± 0.01 vs. 0.38 ± 0.01), representing the better capacity to encourage neovascularization. The Cx43 mRNA expression in each group matched that of VEGF, confirming the results of immunofluorescence (Figure SI 4E). In the MI group, the expression of Bax (1.01 ± 0.01 vs. 1.68 ± 0.01) and Caspase 3 (0.97 ± 0.01 vs. 1.41 ± 0.01) increased, while Bcl2 (1.11 ± 0.01 vs. 0.43 ± 0.01) decreased (Figure SI 4 F). The hydrogel treatment group with the strongest apoptosis inhibitor was Exo/Hydro/AuNPs/CAT. The results indicate that composite hydrogel intramyocardial injection can increase angiogenesis,

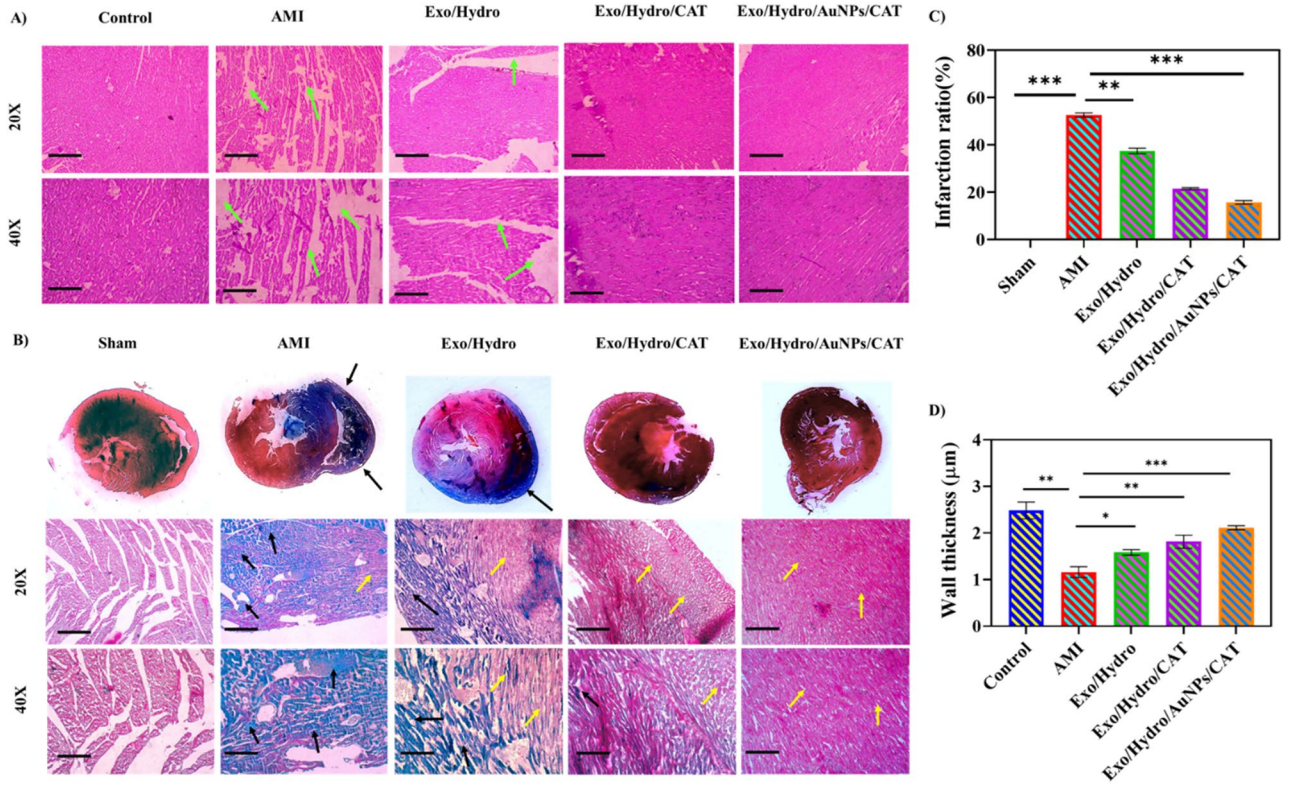

Fig. 8 Evaluation of morphology of the infarcted area reduction and myocardial function after 28 days of surgery. (**A**) Heart sectioning images by H&E staining of control, AMI, Exo/Hydro, Exo/Hydro/CAT, and Exo/Hydro/AuNPs/CAT at various regions with different magnifications, the infarcted sites have been marked with an arrow (green). (**B**) Representative photomicrographs of Masson -stained myocardium of control, AMI, Exo/Hydro, Exo/Hydro/CAT, and Exo/Hydro/AuNPs/CAT with different magnifications, infarcted region with collagen buildup, and the healthy myocardium has been marked with black and yellow arrow respectively. (scale bar = 50 μM for 20X, and 20μM for 40X). *$p < 0.05$, **$p < 0.01$, ***$p < 0.001$

enhance electrical signal transmission, and block cell apoptosis and necrosis, delaying ventricular remodeling and restoring cardiac function.

Discussion

The present study designed an oxygen release system to save cardiac cells and aid cardiac repair after an MI. The persistent oxygen release improved cardiac cell survival by oxygenating them continuously. Current oxygen delivery technologies, such hyperbaric oxygen therapy, cannot manage heart tissue oxygen release. This is because tissue oxygen content decreases promptly following therapy. Specifically, the oxygen delivery device targeted infarcted tissue [39]. Localized oxygen delivery has various advantages over systemic oxygen administration, including increased tissue oxygen content. Oxygen delivery to infarcted hearts relies on blood circulation. Cardiac tissue affected with MI has inadequate vascularization. In tissue engineering, optimal oxygen supply affects cell viability, growth, and function. Myocardial infarction makes it difficult for oxygen availability in the tissues [40]. Infarction and ischemia damage heart tissue, making transplanted cells undesirable [41]. Our study found that producing O_2 can reduce cardiac cell necrosis from hypoxia. This is accomplished by increasing oxygen availability to mimic an infarcted heart. This oxygen deficiency damages tissue and can kill cardiac muscle cells. Myocardial infarction treatment typically involves medication, blood flow restoration, and heart transplantation. A new oxygen-generating hydrogel therapy for myocardial infarction shows potential therapeutic effect.

AuNPs' electrical conductivity and low cytotoxicity make them attractive in cardiac tissue engineering [42]. Katsuhiro Hosoyama et al. developed biocompatible and conductive collagenous-nanometal hybrids for cardiac tissue engineering [43]. Dvir T et al. have reported Au nanowires in alginate scaffolds bridge resistance holes and increase electrical conductivity between cardiomyocytes [44]. Dae et al. developed a framework using conductive Au nanorods to enhance cell retention, diffusion, cardiac cell survival, maturation, cell-cell coupling, and tissue-level synchronized pulsation [45]. In this study, the synergy between CAT and AuNPs created a hydrogel with higher conductivity than normal myocardial tissue, leading to increased Cx43 expression in the infarcted rat heart and thereby enhancing cell-cell communication and electrical coupling. Specifically, CAT is the main

driver of Cx43 expression, while AuNPs further enhance its activity, leading to elevated Cx43 levels.

As reported earlier, after injection into the injured heart, O_2-generating hydrogel releases oxygen to aid tissue healing and regeneration. The hydrogel reduces heart tissue damage from ischemia and reperfusion injury by supplying localized oxygen. Oxygen-generating hydrogels may improve myocardial infarction outcomes and cardiac tissue regeneration. This CAT oxygen release mechanism has advantages over fluorinated substances, H_2O_2 (without complexing), CaO_2, and MgO_2 [46–48]. A notable benefit of this CAT-loaded oxygen-generating technology is extended-release time over a month. The aforementioned mechanisms typically release oxygen for two weeks or less. However, our system released oxygen for four weeks. Additionally, CAT quickly converts H_2O_2 into oxygen, making the system safer without causing cell damage by H_2O_2. Oxygen release systems using CaO_2, MgO_2, and H_2O_2 without complex formation create free H_2O_2 for oxygen production through decomposition. Unlike CaO_2 and MgO_2-based oxygen-generating methods, our approach does not release Ca^{2+} or Mg^{2+} as a by-product, which might cause irregular ion transients in cardiac tissue and make them unsuitable for therapy [49]. As reported elsewhere, GelMA hydrogel scaffold with cardiomyocytes and CaO_2 improved hypoxia cell survival and function [50]. In another study, GelMA hydrogel and CaO_2 bio ink were used to print skeletal muscle tissues. Oxygen-generating substance increased mouse-derived C2C12 myoblast metabolic activity, proliferation, and viability. This study found that released oxygen can cause vasculogenesis in ischemia [51]. After a myocardial infarction (MI), TGF-β expression rises, leading to cardiac fibroblast differentiation into myofibroblasts in a hypoxic setting and ultimately this process creates scar tissues [52].

Adult cardiomyocytes, which contract and pump the heart, have limited regeneration ability. After a myocardial infarction, non-contractile scar tissue replaces destroyed cardiomyocytes, reducing heart function and possibly causing heart failure [53]. Hydrogel may improve cardiomyocyte mitotic behavior and stem cell treatment. Hydrogel supports stem cell development into cardiomyocytes. As previously observed, stem cells on hydrogel scaffolds boost cardiomyocyte mitotic behavior, promoting myocardial growth and regeneration. The hydrogel may increase cardiomyocyte mitotic behavior and regeneration capacity in severely injured myocardium by creating a favorable microenvironment [54]. Meanwhile, injectable hydrogels are attractive regenerative medicine tools because they support and increase biological processes. Previously, O_2-generating hydrogels were found to promote cardiomyocyte karyokinesis and cytokinesis, crucial for cell division and proliferation. Cardiomyocytes can duplicate their genetic material and divide into two daughter cells via karyokinesis and cytokinesis on hydrogel scaffolds in vitro [55]. These mechanisms are essential for heart tissue growth and regeneration, making hydrogel scaffolds useful in cardiac tissue engineering. This method improves cardiomyocyte functioning, viability, and karyokinesis, and cytokinesis. The hydrogel scaffold supports and mimics cell-cell and cell-ECM interactions, allowing cardiomyocytes to align and organize for synchronized contractile performance [56]. The macrophage phenotypic change during tissue healing is important. The pro-inflammatory M1 macrophages that emerge shortly after damage must eventually become anti-inflammatory or pro-healing M2 macrophages for optimal tissue recovery. This phase of transition reduces chronic inflammation and fibrosis, making it advantageous. Post-myocardial infarction macrophage characteristics were examined one week after surgery. At this time linked to reduced inflammation and faster tissue healing, assuming normal tissue repair and regeneration [2, 52]. Oxygen is crucial for saving cardiac cells in infarcted cardiac tissue due to inadequate blood perfusion and insufficient oxygen. However, maintaining oxygen flow to AMI-affected hearts is difficult. Clinical hyperbaric oxygen therapy has poor long-term efficacy in oxygenating tissue. Until revascularization is completed, vascularization techniques struggle to save cardiac cells in infarcted heart tissue. The AMI phase is critical for oxygen delivery to heart cell regeneration. Developing a non-invasive oxygen supply system that releases oxygen regularly would be very feasible and give practical application [57].

This work demonstrates the benefits of immediately injecting an injectable hydrogel composed of degradable Alginate/Fibrin, stem cells derived exosome, O_2-generating CAT, and electrical conductivity enhancer AuNPs at the post-MI site. Co-administration of MSCs-derived Exosomes proved effective in maintaining cardiac function, both immediately and one week after MI, with comparable results. A treatment window of at least one week was found in this study. Rapid therapy after AMI is less clinically viable than this time. The combo treatment's benefits might decrease after 4 weeks after myocardial infarction. However, ventricular remodeling in rats is nearly complete within four weeks of AMI, making it unlikely [58]. Oxygen availability is increased to replicate myocardial infarction settings. Reducing cell necrosis is important because it harms nearby cells and tissues, causing a sterile inflammatory reaction and implant failure. Thus, Exo/Hydro/CAT and Exo/Hydro/AuNPs/CAT hydrogel's oxygen-generating tendencies are likely to improve tissue engineering by inhibiting hypoxic stress, apoptosis, and necrosis-induced cell and tissue damage [41, 59].

Conclusion

In summary, a novel blended hydrogel with (ADMSCs-derived exosomes, catalase (CAT), and AuNPs were successfully synthesized. This novel formulation efficiently removed ROS and produced O_2. The hydrogel effectively scavenged ROS and produced O_2 during hypoxia and inflammation. The hydrogel has a suitable electrical conductivity and high availability. Thus, it controlled AMI-related unhealthy tissue microenvironments. By reducing hypoxic stress, an Exo-loaded hydrogel that creates oxygen improves heart cell survival and proliferation. This study found that O_2-generating hydrogel cohorts reduce hypoxia-induced cell death by limiting apoptosis and necrosis. In vivo experiments on rats with AMI showed that the hydrogel successfully reduced oxygen-related free radicals, hypoxia, TNF-α levels, cell apoptosis, and increased M2/M1 macrophage ratio. In vivo results showed that the hydrogel can restore vital heart functions, reduce infarcted area, and promote angiogenesis. Our hydrogel groups provide promising therapeutic effects in AMI models due to their appropriate cell compatibility in vitro and effective therapeutic impact in vivo. It needs more research and demonstration in big animal models before therapeutic usage.

Supplementary Information

The online version contains supplementary material available at https://doi.org/10.1186/s12951-025-03289-y.

Supplementary Material 1

Acknowledgements
None.

Author contributions
Zhaoyan Xu, Wanzi Hong, Yuanxi Mo, Fen Shu- Supported with synthesis, Characterization, Molecular and biochemical analysis, Yaoxin Liu, Yuqi Cheng, Ning Tan - Data curation, Formal analysis, and Validation.Lei Jiang -Helped with supervised the research.

Funding
This study was supported by Natural Science Foundation of Guangdong Province (Grant no. 2023B1515020082). The work was not funded by any industry sponsors.

Data availability
No datasets were generated or analysed during the current study.

Declarations

Competing interests
The authors declare no competing interests.

Consent to participate
All of the authors agree to work on this project.

Consent for publication
The approval of each author to publish the manuscript has been obtained. The manuscript is not currently under review by any other journal and has not been published before.

Author details
[1]Department of Cardiology, Guangdong Provincial People's Hospital (Guangdong Academy of Medical Sciences), Southern Medical University, Guangzhou 510080, China
[2]Department of Cardiology, The First People's Hospital of Foshan, Foshan 528000, China

Received: 3 December 2024 / Accepted: 2 March 2025
Published online: 17 March 2025

References

1. Rufaihah AJ, Yasa IC, Ramanujam VS, Arularasu SC, Kofidis T, Guler MO, Tekinay AB. Angiogenic peptide nanofibers repair cardiac tissue defect after myocardial infarction. Acta Biomater. 2017;58:102–12. https://doi.org/10.1016/j.actbio.2017.06.009.
2. Su T, Huang K, Daniele MA, Hensley MT, Young AT, Tang J, Allen TA, Vandergriff AC, Erb PD, Ligler FS, Cheng K. Cardiac stem cell patch integrated with microengineered blood vessels promotes cardiomyocyte proliferation and neovascularization after acute myocardial infarction. ACS Appl Mater Interfaces. 2018;10:33088–96. https://doi.org/10.1021/acsami.8b13571.
3. Zhang Y, Zhang J, Butler J, Yang X, Xie P, Guo D, Wei T, Yu J, Wu Z, Gao Y, Han X. Contemporary epidemiology, management, and outcomes of patients hospitalized for heart failure in China: results from the China heart failure (China-HF) registry. J Card Fail. 2017;23(12):868–75. https://doi.org/10.1016/j.cardfail.2017.09.014.
4. Baman JR, Ahmad FS. Heart failure. JAMA. 2020;324(10):1015.
5. Xue K, Zhang J, Li C, Li J, Wang C, Zhang Q, Chen X, Yu X, Sun L, Yu X. The role and mechanism of transforming growth factor beta 3 in human myocardial infarction-induced myocardial fibrosis. J Cell Mol Med. 2019;23:4229–43. https://doi.org/10.1111/jcmm.14313.
6. Ding J, Yao Y, Li J, Duan Y, Nakkala JR, Feng X, Cao W, Wang Y, Hong L, Shen L, Mao Z, Zhu Y, Gao C. A reactive oxygen species scavenging and O2 generating injectable hydrogel for myocardial infarction treatment *in vivo*. Small. 2020;16. https://doi.org/10.1002/smll.202005038.
7. Guan Y, Niu H, Wen J, Dang Y, Zayed M, Guan J. Rescuing cardiac cells and improving cardiac function by targeted delivery of oxygen-releasing nanoparticles after or even before acute myocardial infarction. ACS Nano. 2022;16:19551–66. https://doi.org/10.1021/acsnano.2c10043.
8. Fan Z, Xu Z, Niu H, Gao N, Guan Y, Li C, Dang Y, Cui X, Liu XL, Duan Y, Li H, Zhou X, Lin PH, Ma J, Guan J. An injectable oxygen release system to augment cell survival and promote cardiac repair following myocardial infarction. Sci Rep. 2018;8:1–22. https://doi.org/10.1038/s41598-018-19906-w.
9. Ding J, Yao Y, Li J, Duan Y, Nakkala JR, Feng X, Cao W, Wang Y, Hong L, Shen L, Mao Z, Zhu Y, Gao C. A reactive oxygen species scavenging and O2 generating injectable hydrogel for myocardial infarction treatment *in vivo*. Small. 2020;16:1–9. https://doi.org/10.1002/smll.202005038.
10. Wu T, Liu W. Functional hydrogels for the treatment of myocardial infarction. NPG Asia Mater. 2022;14. https://doi.org/10.1038/s41427-021-00330-y.
11. Wang W, Tan B, Chen J, Bao R, Zhang X, Liang S, Shang Y, Liang W, Cui Y, Fan G, Jia H, Liu W. An injectable conductive hydrogel encapsulating plasmid DNA-eNOs and ADSCs for treating myocardial infarction. Biomaterials. 2018;160:69–81. https://doi.org/10.1016/j.biomaterials.2018.01.021.
12. Yang Y, Liu Y, Chen S, Cheong KL, Teng B. Carboxymethyl β-cyclodextrin grafted carboxymethyl Chitosan hydrogel-based microparticles for oral insulin delivery. Carbohydr Polym. 2020;246:116617. https://doi.org/10.1016/j.carbpol.2020.116617.
13. Chow A, Stuckey DJ, Kidher E, Rocco M, Jabbour RJ, Mansfield CA, Darzi A, Harding SE, Stevens MM, Athanasiou T. Human induced pluripotent stem cell-derived cardiomyocyte encapsulating bioactive hydrogels improve rat heart function post myocardial infarction. Stem Cell Rep. 2017;9:1415–22. https://doi.org/10.1016/j.stemcr.2017.09.003.
14. Kalishwaralal K, Jeyabharathi S, Sundar K, Selvamani S, Prasanna M, Muthukumaran A. A novel biocompatible chitosan–selenium nanoparticles (SeNPs) film with electrical conductivity for cardiac tissue engineering application. Mater Sci Eng C. 2018;92:151–60. https://doi.org/10.1016/j.msec.2018.06.036.
15. Ruschitzka F, Abraham WT, Singh JP, Bax JJ, Borer JS, Brugada J, Dickstein K, Ford I, Gorcsan J 3rd, Gras D, Krum H, Sogaard P, Holzmeister J, R. C. T.S.G. Echo, Cardiac-resynchronization therapy in heart failure with a narrow QRS complex, new engl. J Med. 2013;369:1395–405.

16. Zhang J, Ma A, Shang L. Conjugating existing clinical drugs with gold nanoparticles for better treatment of heart diseases. Front Physiol. 2018;9:642.
17. Shafiq M, Chen Y, Hashim R, He C, Mo X, Zhou X. Reactive oxygen species-based biomaterials for regenerative medicine and tissue engineering applications. Front Bioeng Biotechnol. 2021;9:1–9. https://doi.org/10.3389/fbioe.2021.821288.
18. Shafiq M, Zhang Y, Zhu D, Zhao Z, Kim DH, Kim SH, Kong D. In situ cardiac regeneration by using neuropeptide substance P and IGF-1 C peptide eluting heartpatches. Regen Biomater. 2018;5:303–16. https://doi.org/10.1093/rb/rby021.
19. Chen J, Zhan Y, Wang Y, Han D, Tao B, Luo Z, Ma S, Wang Q, Li X, Fan L, Li C, Deng H, Cao F. Chitosan/silk fibroin modified nanofibrous patches with mesenchymal stem cells prevent heart remodeling post-myocardial infarction in rats. Acta Biomater. 2018;80:154–68. https://doi.org/10.1016/j.actbio.2018.09.013.
20. Xu G, Wang X, Deng C, Teng X, Suuronen EJ, Shen Z, Zhong Z. Injectable biodegradable hybrid hydrogels based on thiolated collagen and oligo(acryloyl carbonate)-poly(ethylene glycol)-oligo(acryloyl carbonate) copolymer for functional cardiac regeneration. Acta Biomater. 2015;15:55–64. https://doi.org/10.1016/j.actbio.2014.12.016.
21. Waters R, Alam P, Pacelli S, Chakravarti AR, Ahmed RPH, Paul A. Stem cell inspired secretome-rich injectable hydrogel to repair injured cardiac tissue. ActaBiomater. 2018;69:95–106. https://doi.org/10.1016/j.actbio.2017.12.025.
22. Fakhrali M, Tamimi D, Semnani H, Salehi A, Ghodsi S, Rajabi M, Pezeshki-Modaress SV, Ebadi S, Abdi M, Ghane. Electroconductive nanofiber/myocardium gel scaffolds applicable for myocardial infarction therapy. ACS Appl Polym Mater. 2024;10:5593–607. https://doi.org/10.1021/acsapm.3c02931.
23. Tamimi M, Rajabi S, Pezeshki-Modaress M. Cardiac ECM/chitosan/alginate ternary scaffolds for cardiac tissue engineering application. Int J Biol Macromol. 2020;164:389–402. https://doi.org/10.1016/j.ijbiomac.2020.07.134.
24. Xuejing, Yu. Application of hydrogels in cardiac regeneration. Cardiol Ther. 2023;12:637–74. https://doi.org/10.1007/s40119-023-00339-0.
25. Lakshmanan R, Kumaraswamy P, Krishnan UM, Sethuraman S. Engineering a growth factor embedded nanofiber matrix niche to promote vascularization for functional cardiac regeneration. Biomaterials. 2016;97:176–95. https://doi.org/10.1016/j.biomaterials.2016.02.033.
26. Montazeri L, Kowsari-Esfahan R, Pahlavan S, Sobat M, Rabbani S, Ansari H, Varzideh F, Barekat M, Rajabi S, Navaee F, Bonakdar S, Renaud P, Braun T, Baharvand H. Oxygen-rich environment ameliorates cell therapy outcomes of cardiac progenitor cells for myocardial infarction. Mater Sci Engineering: C. 2021;121:111836. https://doi.org/10.1016/j.msec.2020.111836.
27. Wu Y, Chang T, Chen W, Wang X, Li J, Chen Y, Yu Y, Shen Z, Yu Q, Zhang Y. Release of VEGF and BMP9 from injectable alginate based composite hydrogel for treatment of myocardial infarction. Bioact Mater. 2021;6:520–8. https://doi.org/10.1016/j.bioactmat.2020.08.031.
28. An Z, Tian J, Liu Y, Zhao X, Yang X, Yong J, Liu L, Zhang L, Jiang W, Song X, Zhang H. Exosomes as a cell-free therapy for myocardial injury following acute myocardial infarction or ischemic reperfusion. Aging Dis. 2022;13:1770–86. https://doi.org/10.14336/AD.2022.0416.
29. Chu DK, Kim LHY, Young PJ, Zamiri N, Almenawer SA, Jaeschke R, Szczeklik W, Schünemann HJ, Neary JD, Alhazzani W. Mortality and morbidity in acutely ill adults treated with Liberal versus Conservative oxygen therapy (IOTA): a systematic review and meta-analysis. Lancet. 2018;391:1693–705. https://doi.org/10.1016/S0140-6736(18)30479-3.
30. Li L, Wang Y, Guo R, Li S, Ni J, Gao S, Gao X, Mao J, Zhu Y, Wu P, Wang H, Kong D, Zhang H, Zhu M, Fan G. Ginsenoside Rg3-loaded, reactive oxygen species-responsive polymeric nanoparticles for alleviating myocardial ischemia reperfusion injury. J Control Release. 2020;317:259–72. https://doi.org/10.1016/j.jconrel.2019.11.032.
31. Liu H, Zhang M, Shi M, Zhang T, Lu W, Yang S, Li Z. Adipose-derived mesenchymal stromal cell-derived exosomes promote tendon healing by activating both SMAD1/5/9 and SMAD2/3. Stem Cell Res Ther. 2021;12(1):338. https://doi.org/10.1186/s13287-021-02410-w.
32. Kim DK, Kang B, Kim OY, Choi DS, Lee J, Kim SR, Go G, Yoon YJ, Kim JH, Jang SC, Park KS. EVpedia: an integrated database of high-throughput data for systemic analyses of extracellular vesicles. J Extracell Vesicles. 2013;2:20384–91. https://doi.org/10.3402/jev.v2i0.20384.
33. Huang X, Neretina S, El-Sayed MA. Gold nanorods: from synthesis and properties to biological and biomedical applications. Adv Mater. 2009;21:4880–910.
34. Korf-Klingebiel M, Reboll MR, Klede S, Brod T, Pich A, Polten F, Napp LC, Bauersachs J, Ganser A, Brinkmann E, Reimann I, Kempf T, Niessen HW, Mizrahi J, Schonfeld HJ, Iglesias A, Bobadilla M, Wang Y, Wollert KC. Myeloidderived growth factor (C19orf10) mediates cardiac repair following myocardial infarctionvol 21, pg 140, (2015), Nat. Med., 22 (2016) 446–446.
35. Anversa P, Cheng W, Liu Y, Leri A, Redaelli G, Kajstura J. Apoptosis and myocardial infarction. Basic Res Cardiol. 1998;93:8–12.
36. Michelis KC, Boehm M, Kovacic JC. New vessel formation in the context of cardiomyocyte regeneration–the role and importance of an adequate perfusing vasculature. Stem Cell Res. 2014;13:666–82.
37. Camelliti P, Green CR, LeGrice I, Kohl P. Fibroblast network in rabbit sinoatrial node: structural and functional identification of homogeneous and heterogeneous cell coupling. Circ Res. 2004;94:828–35.
38. Wang W, Tan B, Chen J, Bao R, Zhang X, Liang S, Shang Y, Liang W, Cui Y, Fan G, Jia H, Liu W. An injectable conductive hydrogel encapsulating plasmid DNA-eNOs and ADSCs for treating myocardial infarction. Biomaterials. 2018;160:69–81.
39. Ding H, Ding J, Liu Q, Lin J, He M, Wu X, Chen X, Xiao C, Ren T, Zhu Y, Gao C, Hu X, Wang J. Mesenchymal stem cells encapsulated in a reactive oxygen species-scavenging and O2-generating injectable hydrogel for myocardial infarction treatment. Chem Eng J. 2022;433:133511. https://doi.org/10.1016/j.cej.2021.133511.
40. Gao H, Liu S, Qin S, Yang J, Yue T, Ye B, Tang Y, Feng J, Hou J, Danzeng D. Injectable hydrogel-based combination therapy for myocardial infarction: a systematic review and meta-analysis of preclinical trials. BioMed Cent. 2024. https://doi.org/10.1186/s12872-024-03742-0.
41. Doescher C, Thai A, Cha E, Cheng PV, Agrawal DK, Thankam FG. Intelligent hydrogels in myocardial regeneration and engineering. Gels. 2022;8. https://doi.org/10.3390/gels8090576.
42. Khlebtsov N, Dykman L. Biodistribution and toxicity of engineered gold nanoparticles: a review of *in vitro* and *in vivo* studies. Chem Soc Rev. 2011;40:1647–71.
43. Hosoyama K, Ahumada M, McTiernan CD, Davis DR, Variola F, Ruel M, Liang W, Suuronen EJ, Alarcon EI. Nanoengineered electroconductive collagenbased cardiac patch for infarcted myocardium repair. ACS Appl Mater Interfaces. 2018;10:44668–77.
44. Dvir T, Timko BP, Brigham MD, Naik SR, Karajanagi SS, Levy O, Jin H, Parker KK, Langer R, Kohane DS. Nanowired three-dimensional cardiac patches. Nat Nanotechnol. 2011;6:720–5.
45. Pena B, Maldonado M, Bonham AJ, Aguado BA, Dominguez-Alfaro A, Laughter M, Rowland TJ, Bardill J, Farnsworth NL, Alegret Ramon N, Taylor MRG, Anseth KS, Prato M, Shandas R, McKinsey TA, Park D, Mestroni L. Gold Nanoparticle-Functionalized reverse thermal gel for tissue engineering applications. ACS Appl Mater Interfaces. 2019;11:18671–80.
46. X. Lu, S. Shi, H. Li, E. Gerhard, Z. Lu, X. Tan, W. Li, K.M. Rahn, D. Xie, G. Xu, F. Zou, X. Bai, J. Guo, J. Yang, Magnesium oxide-crosslinked low-swelling citrate-based mussel-inspired tissue adhesives, Biomaterials 232 (2020) 119719, https://doi.org/10.1016/j.biomaterials.2019.119719.
47. Park S, Park KM. Hyperbaric oxygen-generating hydrogels. Biomaterials. 2018;182:234–44. https://doi.org/10.1016/j.biomaterials.2018.08.032.
48. Choi J, Hong G, Kwon T, Lim JO. Fabrication of oxygen releasing scaffold by embedding H2O2-PLGA microspheres into alginate-based hydrogel sponge and its application for wound healing. Appl Sci. 2018;8. https://doi.org/10.3390/app8091492.
49. Abdel-Mageed HM, Abd El Aziz AE, Abdel Raouf BM, Mohamed SA. Antioxidant-biocompatible and stable catalase-based gelatin–alginate hydrogel scaffold with thermal wound healing capability: immobilization and delivery approach. 3 Biotech. 2022;12:1–12. https://doi.org/10.1007/s13205-022-03131-4.
50. Seyedmahmoud R, Çelebi-Saltik B, Barros N, Nasiri R, Banton E, Shamloo A, Ashammakhi N, Dokmeci RM, Ahadian S. Three-dimensional Bioprinting of functional skeletal muscle tissue using gelatin. Micromachines. 2019;10:1–12.
51. Alemdar N. Oxygen-generating photocrosslinkable hydrogel. Methods Mol Biol. 2018;1771:241–50. https://doi.org/10.1007/978-1-4939-7792-5_19.
52. Wu K, Wang Y, Yang H, Chen Y, Lu K, Wu Y, Liu C, Zhang H, Meng H, Yu Q, Zhang Y, Shen Z. Injectable decellularized extracellular matrix hydrogel containing stromal cell-derived factor 1 promotes transplanted cardiomyocyte engraftment and functional regeneration after myocardial infarction. ACS Appl Mater Interfaces. 2022. https://doi.org/10.1021/acsami.2c16682.
53. Pandey R, Velasquez S, Durrani S, Jiang M, Neiman M, Crocker JS, Benoit JB, Rubinstein J, Paul A, Ahmed RPH. MicroRNA-1825 induces proliferation of adult cardiomyocytes and promotes cardiac regeneration post ischemic injury. Am J Transl Res. 2017;9:3120–37.
54. Williams C, Quinn KP, Georgakoudi I, Black LD. Young developmental age cardiac extracellular matrix promotes the expansion of neonatal cardiomyocytes

in vitro. Acta Biomater. 2014;10:194–204. https://doi.org/10.1016/j.actbio.2013.08.037.
55. Mei JC, Wu AYK, Wu PC, Cheng NC, Tsai WB, Yu J. Three-dimensional extracellular matrix scaffolds by microfluidic fabrication for long-term spontaneously contracted cardiomyocyte culture. Tissue Eng - Part A. 2014;20:2931–41. https://doi.org/10.1089/ten.tea.2013.0549.
56. Shapira-Schweitzer K, Habib M, Gepstein L, Seliktar D. A photopolymerizable hydrogel for 3-D culture of human embryonic stem cell-derived cardiomyocytes and rat neonatal cardiac cells. J Mol Cell Cardiol. 2009;46:213–24. https://doi.org/10.1016/j.yjmcc.2008.10.018.
57. Li J, Lv Y, Zhu D, Mei X, Huang K, Wang X, Li Z, Zhang S, Hu S, Popowski KD, Cheng K, Wang J. Intrapericardial hydrogel injection generates high cell retention and augments therapeutic effects of mesenchymal stem cells in myocardial infarction. Chem Eng J. 2022;427:131581. https://doi.org/10.1016/j.cej.2021.131581.
58. Shen Z, Guo Z, Tan T, Hu J, Zhang Y. Reactive oxygen species scavenging and biodegradable peptide hydrogel as 3D culture scaffold for cardiomyocytes. ACS Biomater Sci Eng. 2020;6:3957–66. https://doi.org/10.1021/acsbiomaterials.0c00340.
59. Zhu Y, Matsumura Y, Velayutham M, Foley LM, Hitchens TK, Wagner WR. Reactive oxygen species scavenging with a biodegradable, thermally responsive hydrogel compatible with soft tissue injection. Biomaterials. 2018;177:98–112. https://doi.org/10.1016/j.biomaterials.2018.05.044.

Publisher's note